# A Data-Adaptive EOF-Based Method for Displacement Signal Retrieval From InSAR Displacement Measurement Time Series for Decorrelating Targets

Rémi Prebet, Yajing Yan, Matthias Jauvin, Emmanuel Trouvé

# A data-adaptive EOF based method for displacement signal retrieval from InSAR displacement measurement time series for decorrelating targets

Rémi Prébet, Yajing Yan, *Member, IEEE,* Matthias Jauvin, Emmanuel Trouvé, *Senior Member, IEEE,*

***Abstract*—In this paper, a data-adaptive method, namely Principal Modes (PM) method, based on the spatially averaged temporal covariance of a time series of InSAR displacement measurement obtained from consecutive SAR acquisitions is proposed to retrieve the displacement signal for decorrelating targets. On wrapped interferogram time series, the PM method can highlight and restore coherent fringe patterns where they are more or less significantly hindered by decorrelation noise, while on unwrapped interferogram time series, the PM method provides a satisfactory separation of the displacement signal from the spatially correlated perturbations. A two stage application of the PM method to both wrapped and unwrapped interferogram time series can significantly improve the retrieval of the displacement signal. Synthetic simulations are first performed to investigate the impact of the choice of the appropriate number of modes to retain in the EOF decomposition and of the time series size on the performance of the PM method, as well as to highlight the efficiency of the PM method. Then, the PM method is applied to time series of wrapped and unwrapped Sentinel 1 A/B interferograms over the Gorner glacier between October 2016 and April 2017. The main characteristics of the PM method, such as realistic assumptions, ease of implementation and high efficiency, are highlighted.**

***Index Terms*—EOF, time series, SAR, interferogram, decorrelating targets**

## I. Introduction

In displacement measurement by SAR imagery, with the arrival of Sentinel 1 A/B images acquired every 6 days over Europe and every 12 days elsewhere, especially with the near real time free access to public, the time series of SAR images has become a unprecedented living subject. A yearly analysis of displacement constitutes the subject of numerous studies of landslide, subsidence, volcano deformation, glacier flow, etc. [1]–[4]. The main contributions of the time series to displacement measurement lie on the follow-up of the temporal displacement evolution and the improvement of the displacement estimation precision. For the former, the time series provides continuous displacement information over time, thus allows for long term monitoring, which is particularly important for natural hazards prediction. For the latter, with advanced multi-temporal techniques (e.g. Permanent Scatterer Interferometry [5]–[8], Small BAseline Subset [9], [10] CAESAR [11], etc), the precision of the displacement rate estimation has been improved significantly, e.g. on the order of 1 mm/yr based on a time series with more than 60 images [12].

Actually, the multi-temporal methods have most been developed for time series of SAR images and focused mainly on targets that stay coherent in all the acquisitions [8], [11]–[17]. In general, these methods use a time series of SAR images to construct a redundant interferometric network. The main idea consists of making use of the redundancy of the interferometric network at the level of wrapped data to filter the interferogram stack. A more or less averaged displacement rate during the time span covered by the time series is estimated after the so called phase linking or phase triangulation [14], [16], [18]. For decorrelating targets, due to rapid surface changes, displacement signal can only be obtained from SAR image pairs with small temporal baselines (i.e. several days or even less). Moreover, low signal to noise ratio (SNR) and data gaps are frequently observed in the displacement measurement, which makes the application of the aforementioned multi-temporal methods impossible for decorrelating targets. Thus, few methods have been documented to deal with time series of displacement measurements for decorrelating targets. A substantial lack of multi-temporal approaches to deal with decorrelating targets becomes obvious, which constitutes the main motivation of this paper.

The Empirical Orthogonal Function (EOF) based analysis [19] is one of the most widely and extensively used methods for time series analysis in atmosphere-ocean science [20], [21]. This family of methods (known also as PCA or Karhunen-Loève decomposition) is mainly a data-adaptive and non-parametric tool, since it does not need an a priori parameter dependent model of the process that generated the time series under analysis. They are primarily designed for the reduction of the dimensionality of a given data set and the compression of a maximum of variance into a minimal number of robust components. The principle of the EOF based methods lies on the construction of the spatial and/or temporal covariance matrix of the time series and the analysis of the latter by eigenvalue decomposition (ED) [19] or singular value decomposition (SVD) [22] in terms of data-based orthogonal functions. It turns out that these orthogonal functions can be classified essentially into trends, oscillatory patterns and noise [23]. Given any space-time geophysical field, EOF based methods find a set of orthogonal spatial (temporal) patterns

R. Prébet is with the LISTIC laboratory at Université Savoie Mont-Blanc, Annecy and École Normale Supérieur Paris-Saclay, Paris, France

Y. Yan, M. Jauvin and E. Trouvé are with the LISTIC laboratory at Université Savoie Mont-Blanc, Annecy, France.

along with a set of associated uncorrelated time (space) series. For many geophysical records, a few leading EOF modes correspond to the record's dominant oscillatory and/or trend modes [20], [23]. They are thus necessary to optimally reconstruct the initial signal. The efficiency of the EOF based methods has been proven in a large number of studies, which helped its widespread use in atmosphere-ocean community. In displacement measurement by SAR imagery, similar analysis has also been adopted in multi-temporal processing chains and in geophysical model inversions. For example, [8] performed a filtering of the interferogram stack by a PCA of the full covariance matrix of the SAR image time series, while in [11], the same analysis was realised to identify the dominant scattering mechanism. In [17], the PCA was used for data compression. [24] and the references therein adopted the PCA in geophysical model inversions. To our knowledge, EOF based analyses have not been applied to InSAR displacement measurement time series.

In this paper, a data-adaptive EOF based method, namely Principal Modes (PM) method, is proposed to retrieve coherent displacement signal from an interferogram time series obtained from consecutive SAR acquisitions for decorrelating targets. The displacement retrieval is performed at two levels: on both unwrapped interferograms (real signal) and wrapped interferograms (complex signal). The PM method is used, in the former case, to separate the displacement signal from the spatially correlated perturbations such as atmospheric residuals; while in the latter case, to restore coherent displacement patterns hindered by decorrelation noise. Synthetic simulations are performed to investigate the appropriate number of modes to retain in the EOF analysis and to highlight the impact of the time series size on the performance of the PM method, as well as to show the efficiency of the PM method. Then, the PM method is applied to a time series of interferograms constructed from consecutive Sentinel-1 A/B acquisitions between October 2016 and April 2017 over the Gorner glacier. The efficiency of the PM method is evaluated by comparisons between the original interferograms and the reconstructions by the PM method.

This paper is organised as follows: in Section II, the principle of the PM method is described in detail. In Section III, synthetic simulations of both unwrapped and wrapped interferogram time series are performed in order to investigate the choice of the appropriate number of modes and the impact of the time series size on the performance of the PM method, also to highlight the efficiency of the PM method. Section IV gives the results of the application of the PM method to time series of Sentinel 1 A/B interferograms over the Gorner glacier. Finally, conclusions and perspectives are given in Section VI.

## II. Methodologies

SAR images are subject to noise of divers origins. Thus, the observed displacement on differential interferograms includes 2 terms: the true displacement signal and different sources of perturbations. The separation between these 2 terms constitutes a major issue in order to obtain the true displacement signal. In case of a time series, this separation can be performed based on different temporal behaviours between the displacement signal and the perturbations, because in most cases, the displacement is temporally and spatially coherent, while the perturbations are not. The use of the EOF based analysis is appropriate to analyse a combination of spatial and temporal trend in a time series in order to find the groups of points (i.e. a spatial pattern) that vary together following a specific time function. In the following, how an EOF based method, the PM method, separates the displacement signal and other perturbations through an analysis of the temporal covariance of a displacement measurement time series is explained in detail.

### A. Mathematical modelling

In case of both wrapped and unwrapped interferograms, each interferogram (i.e. 2D image of interferometric phase) can be represented by a matrix of size $Nl \times Nc$. In order to reduce the dimension of the problem and facilitate the processing later, each interferogram matrix is ordered into a vector, $\phi$, hereafter. Thus,

$$\phi = (\phi_i)_{0 \leq i < Nl \times Nc} \in \mathcal{M}_{Nl \times Nc,1}(\mathbb{R}) \tag{1}$$

On each interferogram, the total signal includes the displacement signal and perturbations. Decorrelation noise and atmospheric perturbations are considered as main error sources on wrapped and unwrapped interferograms respectively [14], [17]. Therefore, in case of unwrapped interferograms, spatially correlated perturbations (atmospheric-like) and random noise are considered; while in case of wrapped interferograms, decorrelation noise is mainly considered (equation 2).

$$\phi = \begin{cases} \phi^d + \phi^a + \phi^b & \phi \in \mathbb{R} \\ \phi^d + \phi^b & \phi \in [0, 2\pi) \end{cases} \tag{2}$$

where $d$ denotes displacement, $a$ spatially correlated perturbations and $b$ random noise.

We now consider a time series of interferograms obtained from consecutive SAR acquisitions, e.g. unwrapped interferogram time series. Assume that we have interferograms at time instants $t_1, t_2, ..., t_N$ and each interferogram includes $\phi_1, \phi_2, ..., \phi_P$ values corresponding to $P$ locations (an ordered set of values from a 2D image). We can order these interferograms in (position, time) way and store them in a matrix, $X$ (hereafter namely data matrix), as shown in equation 3. Thus, a time series of interferograms is represented by a matrix of size $P \times N$. In this way, we can interpret each of the $N$ columns of $X$ as a map for a given time instant and each of the $P$ lines of $X$ as a time series for a given location.

$$X = \begin{pmatrix} \phi_1^1 & \cdots & \phi_1^N \\ \vdots & & \vdots \\ \phi_P^1 & \cdots & \phi_P^N \end{pmatrix} \in \mathcal{M}_{P,N}(\mathbb{R}) \tag{3}$$

In case of wrapped interferogram time series, the data matrix, $X$, is adapted as follows in order to take the phase circularity into account:

$$X = \begin{pmatrix} e^{\phi_1^1} & \cdots & e^{\phi_1^N} \\ \vdots & & \vdots \\ e^{\phi_P^1} & \cdots & e^{\phi_P^N} \end{pmatrix} \in \mathcal{M}_{P,N}(\mathbb{U}) \quad (4)$$

Indeed, this (position, time) way corresponds to the T-mode (time mode) data organisation in PCA analysis. There exists the S-mode (space mode) that arranges the data in (time, position) way and the corresponding data matrix is the transpose of $X$ presented in equation 3 or 4. The selection of T-mode or S-mode depends on the objective of the analysis, more precisely, whether the temporal covariance or the spatial covariance to analyse. The selection of S-mode treats the time series ($N$ times) at each of the $P$ locations as variables in the analysis; the domain is the position, thus the spatial covariance of size $P \times P$ of the time series is analysed. Conversely, the selection of T-mode treats the spatial field, defined by all the $P$ locations at each of the $N$ times as variables; the domain is the time, thus the temporal covariance of size $N \times N$ of the time series is analysed. The spatial covariance characterises the correlation between different positions, thus it is not sensitive to temporal variations. The temporal covariance characterises the correlation between different times, is thus suitable for analysis focused on the temporal evolution of coherent spatial structures. Therefore, T-mode data organisation is adopted in the PM method.

### *B. Covariance matrix construction and analysis*

The temporal covariance of the time series is constructed from the data matrix. We can mention that when working on EOF or covariance, some a priori background field or trend is subtracted from the time series. We remove the mean of all $P$ locations for each time, i.e. the spatial mean, from the data matrix (equation 5). (Note that if the data are organised in S-mode, we remove the mean of each of the $N$ time series for each location, i.e. the temporal mean.) We then obtain the so called data anomaly matrix, $X'$.

$$X' = X - I_n \bar{X} \quad (5)$$

where $I_n$ is a column identity vector with size $P \times 1$.

With

$$\bar{X} = (\bar{X_1}, \bar{X_2}, ..., \bar{X_N}) \quad (6)$$

and

$$\bar{X_j} = \frac{1}{P} \sum_{i=1}^{P} x_{i,j} \quad (7)$$

with $i$, $j$ corresponding respectively to the line and column indices.

Then, the temporal covariance, $R$, is formed from the data anomaly matrix as follows:

$$R = X'^t X' \in \mathcal{M}_{N,N}(\mathbb{C}) \quad (8)$$

where $^t$ denotes the transpose operator of a matrix. In case of wrapped interferogram time series, it is replaced by the trans-conjugate operator in order to obtain a positive hermitian matrix.

To give detailed insight into the temporal covariance matrix, we represent the temporal covariance $R$ in the following way:

$$R = \mathbb{E}[\phi'_m{}^t \phi'_n] \quad (9)$$

where $\phi_n\prime$ is a column of the data anomaly matrix, and $m$ and $n$ correspond to two different times (columns). $\mathbb{E}$ is the mathematical expectation.

Taken into account different contributions in $\phi$ (equation 2), in case of unwrapped interferograms, $R$ becomes

$$R = \mathbb{E}[(\phi'^d_m + \phi'^a_m + \phi'^b_m)^t (\phi'^d_n + \phi'^a_n + \phi'^b_n)] \quad (10)$$

$$= \mathbb{E}[\phi'^{d\,t}_m \phi'^d_n + \phi'^{a\,t}_m \phi'^d_n + \phi'^{b\,t}_m \phi'^d_n + \phi'^{d\,t}_m \phi'^a_n + \phi'^{a\,t}_m \phi'^a_n + \phi'^{b\,t}_m \phi'^a_n + \phi'^{d\,t}_m \phi'^b_n + \phi'^{a\,t}_m \phi'^b_n + \phi'^{b\,t}_m \phi'^b_n] \quad (11)$$

The displacement can be assumed independent of other perturbations, thus $\mathbb{E}[\phi'^{a\,t}_m \phi'^d_n] = 0$ and $\mathbb{E}[\phi'^{b\,t}_m \phi'^d_n] = 0$. For atmospheric-like spatially correlated perturbations, in general, they do not present temporal correlation. However, in the case of displacement measurement from consecutive SAR acquisitions, a common image is shared by the consecutive displacement measurements, therefore, there is a correlation between consecutive times. In what follows,

$$R = \begin{cases} \mathbb{E}[\phi'^{d\,t}_m \phi'^d_n] & |m-n| > 1 \\ \mathbb{E}[\phi'^{d\,t}_m \phi'^d_n + \phi'^{a\,t}_m \phi'^a_n] & |m-n| = 1 \end{cases} \quad (12)$$

In case of wrapped interferograms time series, $R$ becomes

$$R = \mathbb{E}[e^{j(\phi'^d_n - \phi'^d_m + \phi'^b_n - \phi'^b_m)}] \quad (13)$$

$$= \mathbb{E}[e^{j(\phi'^d_n - \phi'^d_m)}] \mathbb{E}[e^{j(\phi'^b_n - \phi'^b_m)}] \quad (14)$$

If $m$ and $n$ are consecutive, similarly, as there is a common image in the formation of the interferogram, strong temporal correlation can exist in the decorrelation noise; otherwise, the decorrelating mechanism of the phenomenon under observation and $\mathbb{E}[e^{j(\phi'^b_n - \phi'^b_m)}] = \gamma_m \gamma_n$ with $\gamma_m$ the interferometric coherence at time $m$ and $\gamma_n$ the interferometric coherence at time $n$. Thus,

$$R = \begin{cases} \gamma_m \gamma_n \mathbb{E}[e^{j(\phi'^d_n - \phi'^d_m)}] & |m-n| > 1 \\ \mathbb{E}[e^{j(\phi'^d_n - \phi'^d_m)}] \mathbb{E}[e^{j(\phi'^b_n - \phi'^b_m)}] & |m-n| = 1 \end{cases} \quad (15)$$

According to equations 12 and 15, in the temporal covariance $R$, after the spatial average, the remaining information is only about the temporal covariance between displacements at times $n$ and $m$ and that of spatially correlated perturbations in case of unwrapped interferograms or that of decorrelation noise in case of wrapped interferograms between consecutive times. The temporal covariance between displacements is continuous (i.e. between all times), while that of the perturbations is not (i.e. only between consecutive times). Since the temporal variation of the displacement and that of the perturbations do not have the same correlation length (i.e. frequency in spectral analysis), it is possible to separate them through a spectral analysis of the temporal covariance [13].

### C. Decomposition of the covariance matrix into variation modes

We apply a SVD[1] to the temporal covariance $R$ and obtain

$$R = UDV^t \tag{16}$$

where $U$ is the left singular vectors of $R$ ($N \times N$ unitary matrix) and its columns $u_i$ are called left singular vectors that form an orthonormal base. $D = diag(\lambda_1, \lambda_2, ..., \lambda_N)$ is a diagonal matrix of singular values in descending order. $V$ is the right singular vectors ($N \times N$ unitary matrix) and its columns $v_i$ are called right singular vectors that form an orthonormal base. Note that in the present case, $U$ and $V$ are identical[2].

Since $R$ is symmetric, it follows[3] that the singular values and the singular vectors (EOFs) decompose $R$ in the following way:

$$R = \lambda_1 u_1 u_1^t + \lambda_2 u_2 u_2^t + ... + \lambda_N u_N u_N^t \tag{17}$$

In equation 17, each term represents an EOF mode. To each EOF mode, correspond two pieces of information: the EOF mode and its importance (how well an EOF mode represents the signal). Each singular vector, $u_i$, corresponds to a temporal EOF. The EOFs are uncorrelated over time, since $u_i$ are orthogonal to each other, hence the name EOF. Its importance is indicated by the corresponding singular value, $\lambda_i$, that provides a measure of the fraction of the total variance in $R$ explained by the EOF mode $i$. This fraction is obtained by dividing $\lambda_i$ by the sum of all singular values. Often, the first few of the $\lambda_i$ dominate the others, from which an optimal reconstruction of the signal can be achieved.

The spatial pattern obtained when an EOF mode is plotted on a map (over $P$ locations) corresponds to the spatial pattern exhibiting a standing variability over time. To see this spatial structure, we calculate

$$a_i = X' u_i \tag{18}$$

with $i = 1, 2, ..., N$.

The components in the vector $a_i$ are the projections of the EOF modes contained in $X'$ on the orthonormal space engendered by $u_i$ and the vector is a map of EOF$_i$. For each EOF mode EOF$_i$, we can find a corresponding $a_i$. These $a_i$ are called principal components (PCs) or expansion coefficients of the EOF which are uncorrelated in space.

### D. Reconstruction with selected modes

We can reconstruct the data anomaly matrix, $X'$, from the singular vectors and the PCs as follows:

$$\hat{X}' = \sum_{i=1}^{N} a_i u_i^t \tag{19}$$

In equation 19, the singular vectors ($u_i$) can be considered as functions of time, while the PCs ($a_i$) functions of space. The former represents the variability modes of all the positions over time, and the latter is there to modulate this variability according to the position in space. By truncating the sum in equation 19 at some $i \ll N$, we only keep the modes of the first (largest) few singular values. The rationale to do so is that the first modes capture the main temporal dynamical behaviours of the signal in the time series and other modes mainly correspond to different sources of perturbations.

The fraction of the total variance is often the basis for deciding the number of EOFs to retain in a given decomposition. A typical choice is to retain those modes that, when summed up, explain 95% of the signal. In case of known data uncertainty, the number of modes to retain can be determined such that the misfits between the reconstruction and the noisy data are, on average, of the order of magnitude of the data uncertainty as proposed in [24]. Moreover, when the statistical characteristics of the noise present in the data are known, a Monte Carlo method that generates random matrices of noise having the same statistical characteristics can help decide when pure noise is likely to be interpreted as a displacement signal if a mode is kept [25].

To reconstruct the data matrix, the spatial average for each time is added back to the reconstructed data anomaly matrix.

$$\hat{X} = I_n \bar{X} + \hat{X}' \tag{20}$$

### E. Perturbations by low SNR

Low SNR always happens to part of or the whole interferogram time series for decorrelating targets. A question, whether the reconstruction is credible, arises when dealing with time series with low or even very low SNR that hinders the structure of the displacement pattern. Of course, if all the interferograms in a time series present low or very low SNR, the PM method cannot learn about the underlying processes that control the evolution of the displacement, then the reconstruction by the PM method cannot be considered reliable. Here, we consider the case where displacement patterns are partially or completely hampered by perturbations on only part of interferograms in a time series and the perturbations do not excessively mask the underlying signal, the remaining interferograms still carry enough information to reconstruct a reasonable version of the time series.

The first question is about the critical number of interferograms with low SNR from which the reconstruction cannot be considered reliable any more. For this, the differences between the reconstructions and the original interferograms of good quality, in other words, the residuals of interferograms of good quality, can provide useful information. If the interferograms of good quality are not degraded by the reconstructions, it implies that even with the presence of an amount of interferograms with low SNR in the time series, the spatial pattern whose magnitude varies over time (observed from the interferograms of high SNR) can be captured and the PM method works.

In case when the PM method works, suppose that $\phi'_m$ and $\phi'_n$, two columns of the data anomaly matrix $X'$, correspond to two interferograms with low and high SNR respectively. From

[1] a ED can also be applied.

[2] The columns of $U$ are a set of orthonormal eigenvectors of $RR^t$ and the columns of $V$ are a set of orthonormal eigenvectors of $R^tR$. $R^tR = RR^t$, thus $U = V$.

[3] This follows from a famous theorem by Hilbert, that is commonly referred to as the spectral representation theorem.

equations 18 and 19 and assume that only one mode is kept in the reconstruction for sake of simplicity, the reconstructed $\phi'_m$ and $\phi'_n$ can be expressed respectively as:

$$\hat{\phi'_m} = \begin{pmatrix} (\phi'_{1,1}U_{1,1} + \ldots + \phi'_{1,N}U_{N,1})U_{m,1} \\ (\phi'_{2,1}U_{1,1} + \ldots + \phi'_{2,N}U_{N,1})U_{m,1} \\ \ldots \\ (\phi'_{P,1}U_{1,1} + \ldots + \phi'_{P,N}U_{N,1})U_{m,1} \end{pmatrix} \quad (21)$$

$$\hat{\phi'_n} = \begin{pmatrix} (\phi'_{1,1}U_{1,1} + \ldots + \phi'_{1,N}U_{N,1})U_{n,1} \\ (\phi'_{2,1}U_{1,1} + \ldots + \phi'_{2,N}U_{N,1})U_{n,1} \\ \ldots \\ (\phi'_{P,1}U_{1,1} + \ldots + \phi'_{P,N}U_{N,1})U_{n,1} \end{pmatrix} \quad (22)$$

A common structure is observed for both $\hat{\phi'_m}$ and $\hat{\phi'_n}$. The only difference lies in the singular vector components $U_{m,1}$ and $U_{n,1}$. Since $U_{m,1}$ and $U_{n,1}$ are different components of $U$, they are thus consistent, i.e. if $U_{n,1}$ is erroneous, so is $U_{m,1}$. Therefore, if $\hat{\phi'_n}$ is a low-pass filtered version of $\phi'_n$ and no bias is detected, it implies that the PM method learned successfully about the underlying displacement signal and the singular vectors $U$ that represent the main variation directions approximate as closely as possible those obtained in case of high SNR. Therefore, the reconstructions of interferograms of low SNR, $\hat{\phi'_m}$, can also be considered as a low-pass filtered version of $\phi'_m$, thus credible.

### *F. Summary of the PM method*

To summarise, the PM method calls for the determination of a mathematical model that captures the essential physical or statistical properties of a displacement measurement time series by considering the signal included in the time series as the sum of a stable average and a series of variation modes (trend, oscillation or random noise) that are orthogonal to each other (equation 23). These modes have a temporal trend and a space varying function.

$$X = \bar{X} + \sum_{i=1}^{N} \mu_i \Phi_i \quad (23)$$

With

$$\mu_i = \frac{\lambda_i}{\sum_j \lambda_j} \quad (24)$$

$$\Phi_i = \begin{cases} \frac{1}{\mu_i} a_i u_i^t \text{ if } \mu_i \neq 0 \\ 0 \text{ else} \end{cases} \quad (25)$$

According to the principle of the PM method, it is particularly suitable for measurement of continuous displacement over time (linear, with acceleration/deceleration, sinusoidal variation, etc). In case of significantly irregular displacement behaviour over time (e.g. intermittent displacement), there will be no dominant variation modes in the decomposition of the temporal covariance matrix and the performance of the PM method will degrade significantly. With continuous displacement over time, on one hand, it can be considered as a temporal filter that has the ability to separate the temporally coherent signals from perturbations that have a chaotic behaviour over time by keeping appropriate number of modes. On the other hand, it can be considered as a gap filler that is capable of reconstructing coherent displacement signal in case of low SNR based on the temporal correlation of spatial patterns present in the displacement time series.

The performance of the PM method also depends on the quality of the sample temporal covariance estimation. In [8], [11], homogeneous pixels are used to estimate the covariance in order to improve the quality of the estimation. This idea can also be applied in the PM method. However, in this way, an interferogram will be divided into several homogeneous areas, with each corresponding to an independent reconstruction possibly with different number of modes. Discontinuities are thus possible between different homogeneous areas. Further investigation will be necessary to highlight the advantages of this approach. Moreover, the number of modes retained in the reconstruction and the number of measurements in the time series also have an impact on the performance of the PM method . The impact of these two factors will be discussed in Section III through synthetic simulations.

## III. SYNTHETIC SIMULATIONS

The performance of the EOF based methods in terms of denoising effects has been proven in numerous studies. However, the choice of the appropriate number of modes to retain in the reconstruction still remains challenging in case without ground truth. Synthetic simulations have thus been performed in order, on one hand, to investigate the impact of the number of modes to retain in the reconstruction and the time series size on the performance of the PM method and on the other hand, to show the efficiency of the PM method.

### *A. Displacement modelling*

Linear displacement with constant velocity, nonlinear displacement with acceleration (or deceleration) and with periodic oscillations (e.g. seasonal variability) are most considered in displacement measurement. Therefore, in the present synthetic simulations, these three types of displacement are considered. However, remind that in the PM method, the EOFs are classified into trend, oscillatory patterns and noise. The linear displacement and the nonlinear displacement with acceleration can indeed be considered as in the class of trend EOF for the PM method. The nonlinear displacement with periodic oscillations corresponds to the class of oscillatory patterns EOF. Therefore, in the following, only the results of the linear displacement (namely trend displacement hereafter) and the nonlinear displacement with oscillations (namely oscillatory displacement hereafter) are illustrated in order to avoid redundancy.

To simulate the trend displacement, an arbitrary displacement model (equation 26), providing spatial and temporal coherent displacement fields, is chosen. In the provided displacement field, the displacement value decreases with the distance from the centre of the field and the value at the centre increases over time. Indeed, it models somehow the birth of a volcano.

$$f(t, r) = (1 - r/2)t \quad (26)$$

where $r$ is the distance from the centre of the field and $t$ is the time from a predefined origin.

The oscillatory displacement is simulated inspiring from the trend displacement model by involving temporal and spatial variations at different scales (i.e. sum of three embedded sinusoidal behaviours, see equation 27) that correspond to complex oscillations. Note that a particularly complex displacement behaviour is chosen here to test the performance of the PM method.

$$f(t,r) = \sin(\frac{\pi}{2}t)\cos(\frac{\pi}{2}r) \; + \; 0.5 \; \cos(\frac{3\pi}{2}t)\cos(5\pi r) + \sin(\frac{5\pi}{2}t)\cos(10\pi r) \tag{27}$$

### B. Perturbation simulation

On real unwrapped interferograms, spatially correlated perturbation such as the turbulent atmospheric noise is considered as the main error source that hinders the displacement signal. This kind of perturbation is characterised by a spatial correlation, but a random behaviour over time. To generate the spatially correlated noise, an auto-correlation function in power form $c(r) = r^{-\beta}$ with $\beta = 1.2$ is used to modulate a standard normal distribution (zero mean and unit standard deviation) in frequency domain. Finally, to tune the SNR, an amplification factor (3, unless otherwise indicated) is multiplied to the thereby generated noise.

On real wrapped interferograms, the decorrelation noise is considered as the main factor that hinders the displacement signal. Therefore, the noise to simulate for wrapped interferograms is the decorrelation noise. For this, we first generate an arbitrary coherence matrix (spatially correlated noise whose values are between 0 and 1) for each time. The decorrelation noise is generated from the coherence matrix according to equation 28 [26].

$$\phi^t_{x,y} \sim \mathcal{N}\left(0, \frac{1}{2M}\frac{1-(\gamma^t_{x,y})^2}{(\gamma^t_{x,y})^2}\right) \tag{28}$$

where $M$ is the number of multi-looking, $M = 2$ unless otherwise indicated. $\gamma^t_{x,y}$ is the coherence at time instant $t$ on position $(x, y)$.

### C. Experiment setup

In the following, both unwrapped and wrapped interferogram time series have been generated from the models of trend and oscillatory displacements mentioned previously. Perturbations corresponding to each type of interferograms are also generated. The spatial and temporal parameters for all simulations are chosen in an arbitrary way, with $P = 500\times500$ and $N = 20$. For each case, three time series, i.e. displacement time series, noise time series and total signal time series, are generated. Then, for each time series, the data matrix, $X$ and the temporal covariance, $R$, are constructed. A SVD is applied to each temporal covariance. Detailed analyses are performed on each decomposition and data reconstruction is carried out by keeping an appropriate number of modes.

### D. Validation metrics

To define a criterion for the selection of an appropriate number of modes, the root mean square deviation (RMSD) is used. It can be calculated as follows:

$$\text{RMSD} = \frac{1}{\bar{\sigma_\Phi}}\sqrt{\frac{\sum_{i=1}^{N}||\hat{\Phi}_i - \Phi_i||^2}{NP}} \tag{29}$$

where $\bar{\sigma_\Phi}$ denotes the temporal mean standard deviation, $\hat{\Phi}_i$ and $\Phi_i$ denote respectively the estimated and the observed (or true) values at each time instant $i$. In case of complex data, $\bar{\sigma_\Phi}$ is replaced by $\bar{\sigma}_{e^{j\Phi}}$, $\hat{\Phi}$ and $\Phi$ are replaced by $e^{j\hat{\Phi}}$ and $e^{j\Phi}$ respectively.

The RMSD is a measure of accuracy and frequently used to measure the difference between values predicted by a model or an estimator and the values actually observed. The RMSD serves to aggregate the magnitudes of the errors in estimation for various time instants into a single measure of estimative power. Note that the RMSD is different from the average error, because the former mixes information concerning average error with information concerning variation in the errors. The effect of each error on the RMSD is proportional to the size of the squared error thus larger errors have a disproportionately large effect on the RMSD [27].

The number of EOF modes that minimises the RMSD is denoted by $imin$ with the associated $\text{RMSD}_{min}$. The RMSD of the noisy data (or original data) is denoted by $\text{RMSD}_{max}$. The error reduction rate, $\tau_{err}$, is defined as

$$\tau_{err} = 1 - \frac{\text{RMSD}_{min}}{\text{RMSD}_{max}} \tag{30}$$

The error reduction rate varies between 0 (no improvement) and 1 (perfect reconstruction). It measures the gain of accuracy with the application of a method, thus indicates the efficiency of the method.

### E. Choice of the appropriate number of modes

Since the fraction of the total variance explained by each mode provides useful information for the decision of the number of modes to retain, the representativity diagram, indicating the percentage of the total variance explained by each mode (expressed as $\lambda_i / \sum_{i=1}^{N}\lambda_i$) is first analysed. The representativity diagrams of the trend and oscillatory displacements in the case of unwrapped interferogram time series are presented in Figure 1 and Figure 2 respectively. The first observation in both cases is that there is no clear complete separation criterion between the displacement signals and the perturbations. Moreover, in both cases, the fraction of the variance of the total signal (Figure 1 and Figure 2) explained by the first mode is dominant and the fraction of the variance of the noise decreases with the increase of the number of modes. In case of trend displacement, the total displacement signal variance can be explained by the first mode, while it is explained by the first three modes in case of oscillatory displacement. According to the representativity diagrams in the present examples, 1 mode and 2 modes are appropriate to retain in the reconstruction for the trend and oscillatory

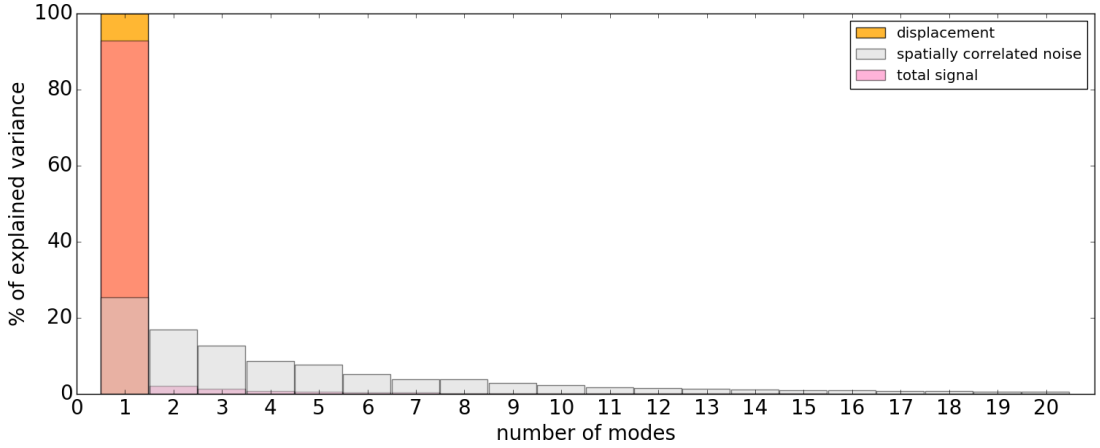


Fig. 1. Representativity diagram of each EOF mode of trend displacement, spatially correlated noise and total signal in case of unwrapped interferogram time series.

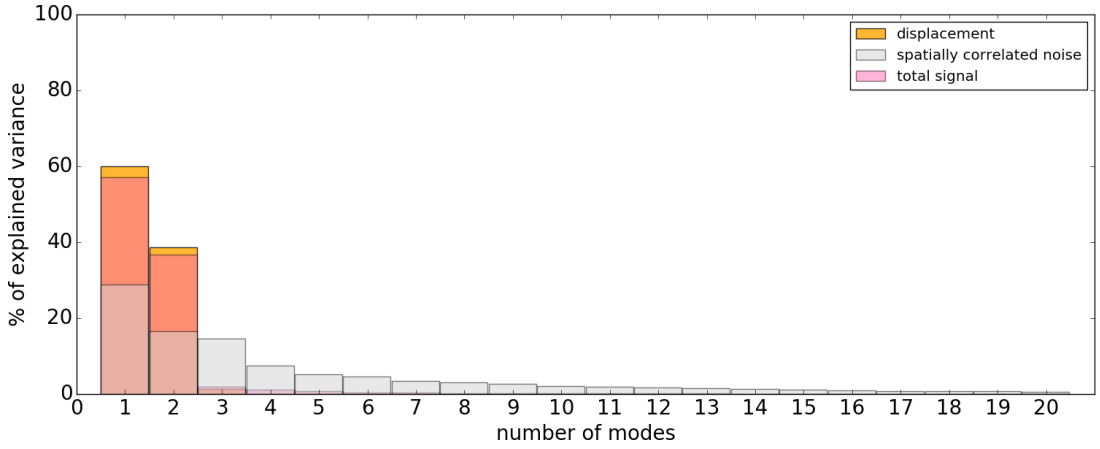


Fig. 2. Representativity diagram of each EOF mode of oscillatory displacement, spatially correlated noise and total signal in case of unwrapped interferogram time series.

displacements respectively, which is further confirmed by the RMSD with respect to the truth (Figure 3 (a) and (b)).

For wrapped interferogram time series, according to the representativity diagrams of the trend and oscillatory displacements shown in Figure 4 and Figure 5 respectively, the displacement signal variability is spread over more modes compared to the cases of unwrapped interferograms, especially in case of oscillatory displacement. Moreover, the fraction of the variance of the noise is uniform for all modes. Therefore, in these two cases, the determination of the number of modes to retain from the representativity diagram of the displacement signal is difficult, and impossible from that of the total signal. Finally, the numbers of modes to retain in these two case are determined based on the RMSD with respect to the truth shown in Figure 3 (c) and (d), thus 2 modes for the trend displacement and 3 modes for the oscillatory displacement.

Note that the numbers of modes to retain aforementioned are obtained from one simulation. In order to verify the stability of the truncation with respect to the random simulations. 500 simulations have been performed. The mean and the standard deviation of the number of modes minimising the RMSD are shown in Table I. According to Table I, the choices of the appropriate number of modes in the 4 aforementioned cases are confirmed. In particular, note that in case of trend displacement, the standard deviation of the $imin$ value is 0 for both wrapped and unwrapped interferogram time series, which implies that the first mode is always sufficient to explain the total displacement variance in case of unwrapped data, while the first two modes in case of wrapped data. Indeed, this conclusion is consistent with observations in most ocean-atmosphere applications. It can thus be used for the choice of the number of modes in real data, given linear displacement characteristics.

| - | $\overline{imin}$ | $\sigma_{imin}$ |
|---|---|---|
| unwrapped trend disp. | 1.0 | 0.0 |
| unwrapped oscillatory disp. | 2.214 | 0.4101 |
| wrapped trend disp. | 2.0 | 0.0 |
| wrapped oscillatory disp. | 2.742 | 0.0083 |

TABLE I
MEAN AND STANDARD DEVIATION OF THE NUMBER OF MODES MINIMISING THE RMSD WITH RESPECT TO THE TRUTH, $imin$, OBTAINED FROM 500 SIMULATIONS.

In most real data case, the ways to determine the appropriate number of modes presented above cannot work any more,

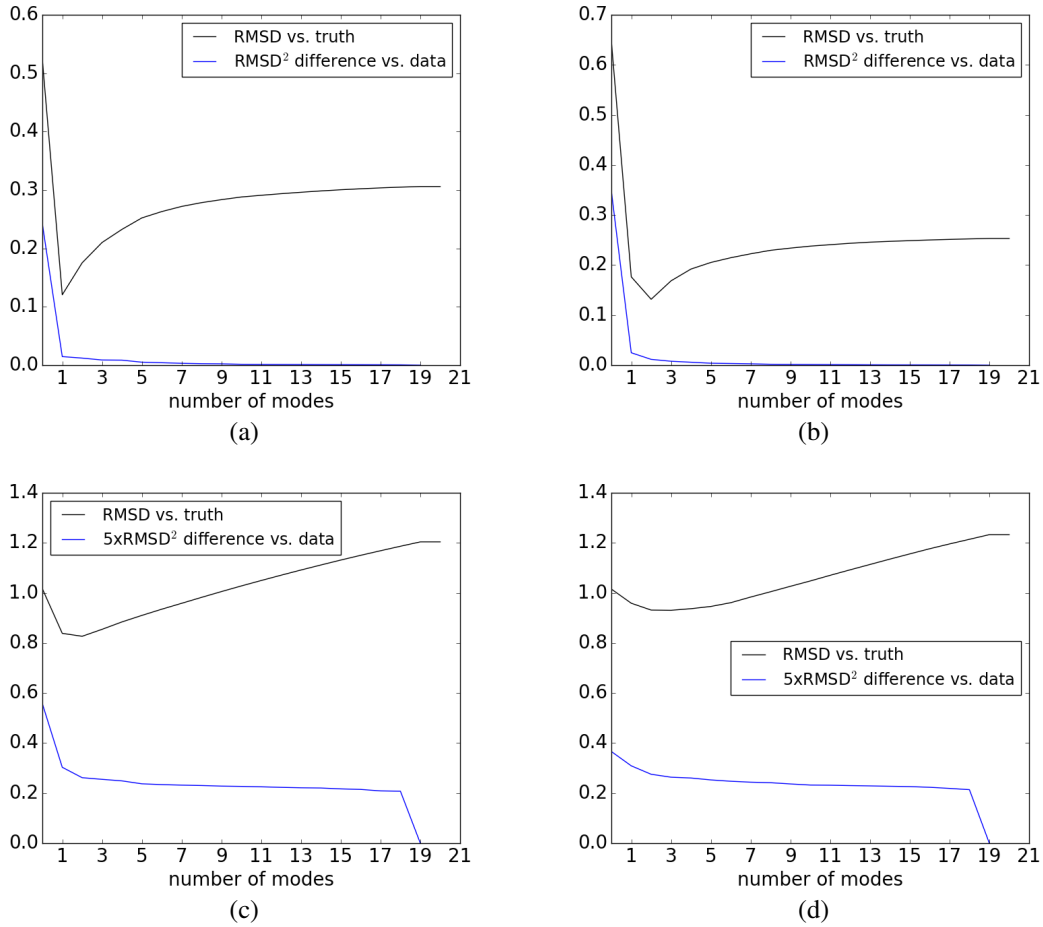


Fig. 3. RMSD with respect to the truth as a function of the number of modes retained in the reconstruction and difference of squared RMSD with respect to the data between consecutive numbers of mode (the value at the position of the number of mode $i$ corresponds to $\text{RMSD}_i^2$ - $\text{RMSD}_{i+1}^2$) for (a) trend displacement (b) oscillatory displacement in case of unwrapped interferogram time series and for (c) trend displacement (d) oscillatory displacement in the case of wrapped interferogram time series. Note that in the case of wrapped displacement, the difference of squared RMSD is multiplied by 5 in order to facilitate the comparison.

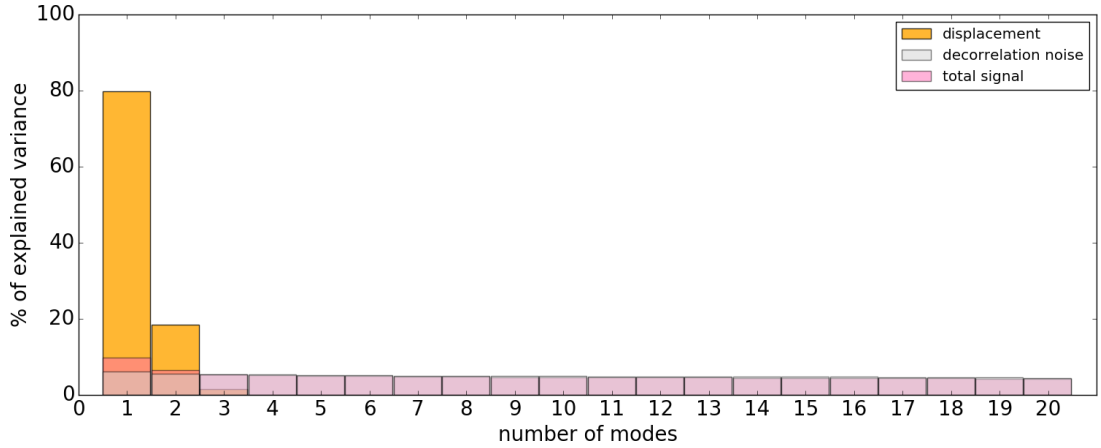


Fig. 4. Representativity diagram of each EOF mode of trend displacement, decorrelation noise and total signal in case of wrapped interferogram time series.

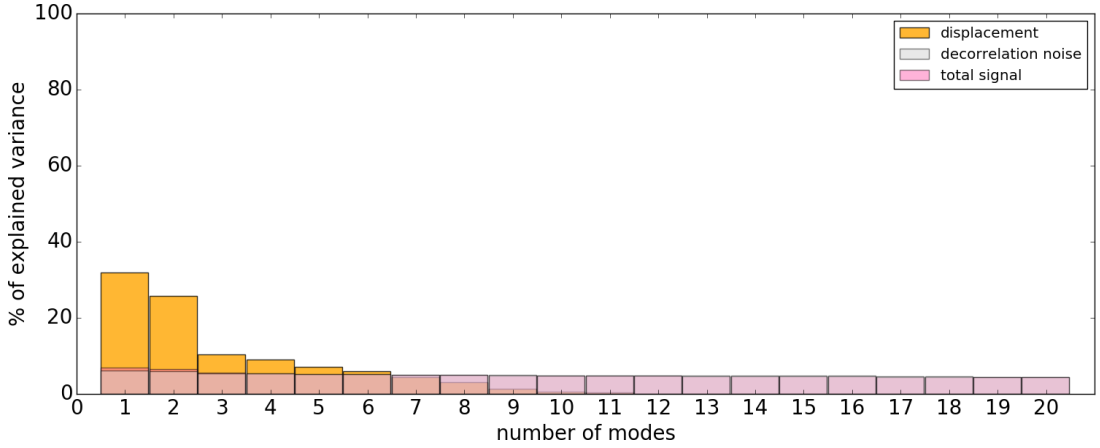


Fig. 5. Representativity diagram of each EOF mode of oscillatory displacement, decorrelation noise and total signal in case of wrapped interferogram time series.

because of the lack of the ground truth or a priori information on the displacement. To deal with the case without information on the data uncertainty, we calculated the squared RMSD of the reconstruction with respect to the noisy data and analysed the difference of the latter between consecutive numbers of mode. In Figure 3, the position at which the RMSD$_{min}$ with respect to the truth is obtained corresponds to the position at which the decrease of the difference of the squared RMSD with respect to the data begins to slow down. In other words, the difference of the squared RMSD with respect to the data begins to slow down when the mode $imin + 1$ is retained. Indeed, when the difference of the squared RMSD with respect to the data between consecutive modes begins to slow down, it implies that the contribution of the additional mode can be neglected and the reconstruction is very close to the data. Given the fact that data uncertainty is present, we do not want the reconstruction is so close to the data, as a result, the appropriate number of mode to retain should be the number of mode before the one with which the difference of the squared RMSD tends to be stable, thus the mode $imin$. Regarding the decrease (to zero) of the squared RMSD difference at the position of the mode 19 in case of wrapped interferogram time series (Figure 3 (c) and (d)), this is because the fraction of the variance explained by each mode between 1 and 19 is similar, but very small by the mode 20, thus the difference of the squared RMSD between 19 modes and 20 modes ($1.0e^{-15}$) is almost zero, while that between 18 modes and 19 modes is on the order of 0.2, hence a noticeable decrease on the squared RMSD difference plot at the position of the mode 19. Note that even though Figure 3 represents one simulation, the same observation is obtained from 500 simulations. Therefore, in real data case, the difference of squared RMSD with respect to the data between consecutive numbers of modes is worth investigation for the choice of modes to retain.

### F. Impact of the time series size

In the previous simulations, the time series size is 20 based on an arbitrary choice. It is interesting to analyse the impact of the time series size in order 1) to get the information about the minimal time series size that allows the PM method getting satisfactory results 2) to know if a large time series size improves or degrades the quality of the reconstruction. For this, simulations with time series size varying between 10 and 100 are performed in case of trend and oscillatory displacements. For each time series size, 500 simulations are performed to avoid randomness.

*1) Unwrapped interferogram time series:* Figure 6 shows the error reduction rate ($\tau_{err}$) and the number of mode with the smallest RMSD ($imin$) as a function of time series size for trend displacement and oscillatory displacement in the case of unwrapped interferogram time series.

The global observation is that increasing time series size does not degrade the quality of the reconstruction. For trend displacement, the first mode is always sufficient to capture the main displacement variability, with increasing time series size. The error reduction rate is increased quickly when the time series size increases from 10 to 30. After that, with further increasing time series size, the error reduction rate continues to increase, but the increase rate slows down. In particular, when the time series size is larger than 50, the gain in error reduction rate is very small. If a $\tau_{err}$ value on the order of 0.5 can be considered as an indicator of good results, then in this case, a time series size of 10 is sufficient. For oscillatory displacement, on average, the first two modes are sufficient to capture the main displacement variability, with increasing time series size. The same as in the previous case, the error reduction rate increases quickly when the time series size increases from 10 to 30, then the increase rate slows down. When the time series size is larger than 40, the gain in error reduction rate is very small. Note that in this case, globally the error reduction rate is smaller than that in the case of trend displacement. A error reduction rate value of 0.5 is reached when the time series size is 70. With a time series size of 10, the error reduction rate is 0.3. Therefore, larger minimal time series size is required in this case to ensure the quality of the reconstruction.

*2) Wrapped interferogram time series:* Figure 7 shows the error reduction rate ($\tau_{err}$) and the number of mode with the smallest RMSD ($imin$) as a function of time series size for

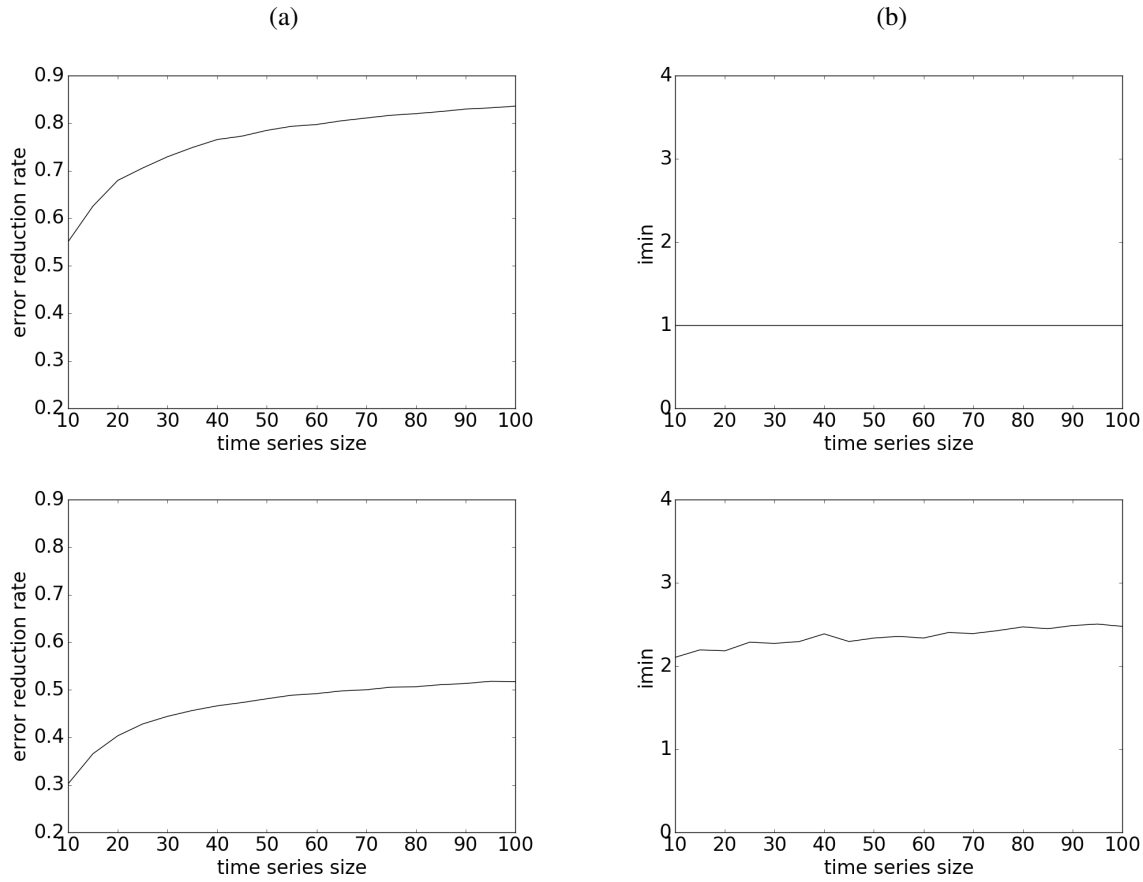


Fig. 6. (a) $\tau_{err}$ and (b) $imin$ as a function of time series size for trend displacement (top) and oscillatory displacement (bottom) in the case of unwrapped interferogram time series.

trend displacement and oscillatory displacement in case of wrapped interferogram time series.

As in the previous case, increasing time series size does not degrade the quality of the reconstruction. Another global observation is that the error reduction rates are smaller than those in the case of unwrapped interferograms. One may consider this as an indicator of a degradation of efficiency of the PM method in this case. According to detailed inspection, this degradation is mainly due to residual decorrelation noise that still exists in the reconstruction. However, with the missing fringes being reconstructed successfully, even though with the presence of residual decorrelation noise, the wrapped interferograms can be unwrapped correctly. Therefore, smaller error reduction rates in this case do not indicate a degradation of the efficiency of the PM method. For trend displacement, the error reduction rate has a behaviour similar to that in the case of unwrapped interferograms. When the time series size is between 10 and 15, only one mode is identified to represent the main displacement variability. Then with larger time series size, two modes are identified and this number stays stable even with further increase of time series size. Therefore, in this case, the minimal time series size should be 15. For oscillatory displacement, the behaviour of the error reduction rate is similar to that of the trend displacement. The $imin$ value increases with increasing time series size. However, note that when the time series size is larger than 50, even with more modes identified, the gain in error reduction rate is very limited. A time series size of about 30 can give satisfactory results.

### G. Efficiency of the PM method

Figure 8 gives an example of the truth, the noisy displacement, the reconstruction by the PM method, the residual (noisy displacement - reconstruction) and the noise included in the noisy displacement for trend and oscillatory displacement in cases of unwrapped and wrapped interferograms time series in order to show the efficiency of the PM method in a qualitative way. The reconstructions are obtained with a number of mode determined from the RMSD. For trend displacement, in both unwrapped (first column) and wrapped (third column) interferograms cases, the displacement patterns hampered by the noise have been reconstructed correctly and the residuals are very similar to the noise present in the noisy displacement. Therefore, in case of trend displacement, the separation between the displacement signal and the noise is very efficient. For oscillatory displacement, the displacement/noise separation efficiency is degraded compared to that for trend displacement because of the complexity of the displacement characteristics. In case of unwrapped interferograms (second column), no displacement signal is identified in the residual but part of spatially correlated perturbations still remain in the reconstruction. In case of wrapped interferograms, the global displace-

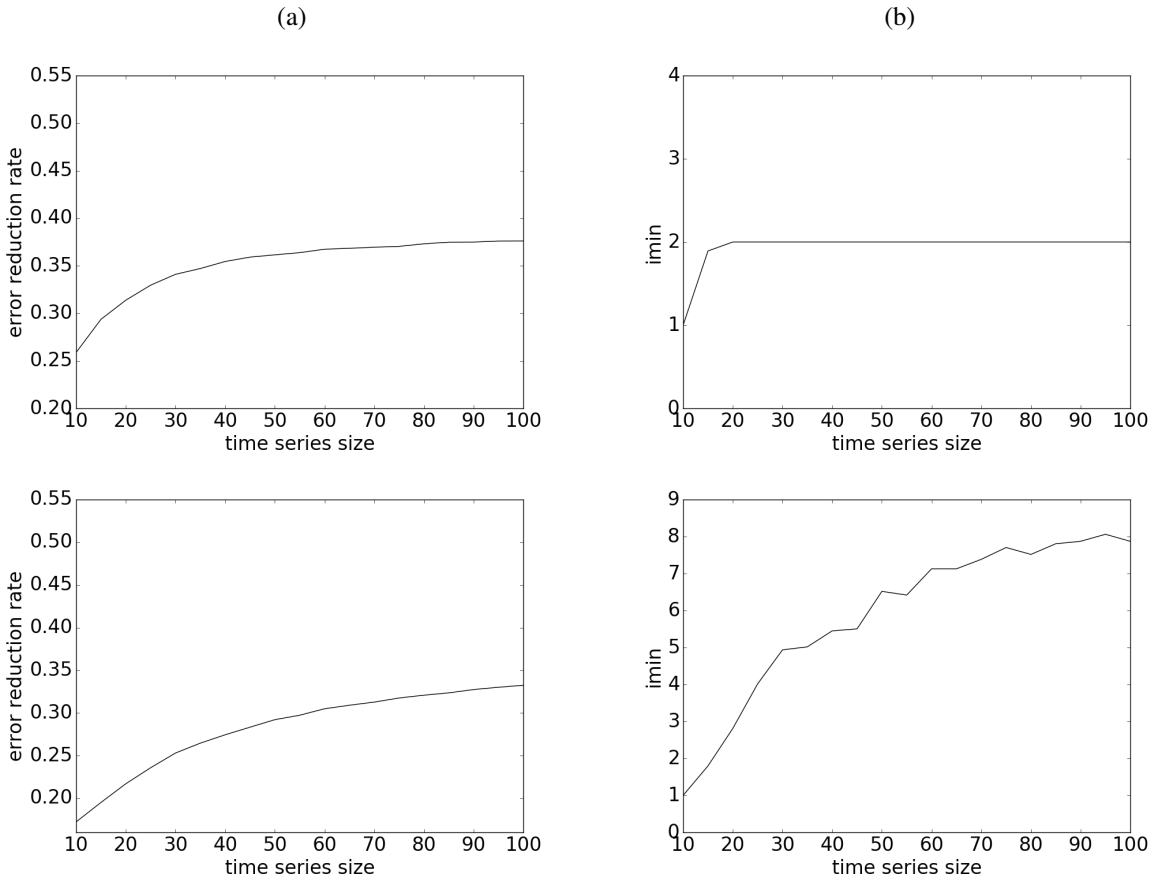


Fig. 7. (a) $\tau_{err}$ and (b) $imin$ as a function of time series size for trend displacement (top) and oscillatory displacement (bottom) in the case of wrapped interferogram time series.

ment pattern has been reconstructed successfully. However, displacement signal is observed in the residual, even though the magnitude is very small. Obviously, keeping more modes in the reconstruction can help get back the displacement signal in the residual at the expense of keeping more noise in the reconstruction at the same time. This strategy thus degrades the quality of the reconstruction. A better approach to get back the displacement signal in the residual without degrading the quality of the reconstruction consists of a further analysis of the residual in terms of spatial/temporal correlation. Note also that the simulated oscillatory displacement corresponds to a very difficult case, i.e. the sum of three embedded sinusoidal behaviours (i.e. product of sine and cosine functions, see equation 27). Indeed, oscillatory displacements from the sum of as many as four single sinusoidal behaviours, the sum of two embedded sinusoidal behaviours and one embedded sinusoidal behaviour have also been simulated. Displacement signal is only observed in the residual for some interferograms in the case with two or three embedded sinusoidal behaviours. These complex displacement behaviours only represent a few particular cases in Earth displacement measurements. Therefore, the PM method can be considered efficient in most applications of Earth displacement measurement.

To give further quantitative analysis results, RMS errors of the reconstruction and noisy data compared to the truth are presented with different noise levels (Figure 9). For both trend and oscillatory displacements in cases of wrapped and unwrapped interferograms time series, the RMS errors of the reconstructions are significantly decreased compared to those of noisy data. In case of unwrapped interferograms, the RMS error reduction is more significant in case of lower SNR; while in case of wrapped interferograms, the RMS error reduction is more efficient in case of higher SNR. According to Figure 9, it can be concluded that the PM method can improve significantly the global accuracy. For individual points, the quality of the reconstruction varies, depending on the noise level on each point as well as the global noise level of the time series. As shown in Figure 10 by examples of displacement time series over a point chosen arbitrarily, in general, the reconstruction gets closer to the truth with the decrease of the global noise level in the four cases and the reconstruction is more accurate for less noisier data sets in a given time series. However, the benefit of the PM method is more important in case of low and moderate SNR, because the gain in accuracy in these cases is crucial to make useless data sets exploitable (left and middle columns in Figure 10).

### *H. Impact of unique events*

In order to highlight the impact of unique events whose displacement pattern is different from those observed in most interferograms in the time series, time series (with 20 interferograms) of a constant displacement pattern have been

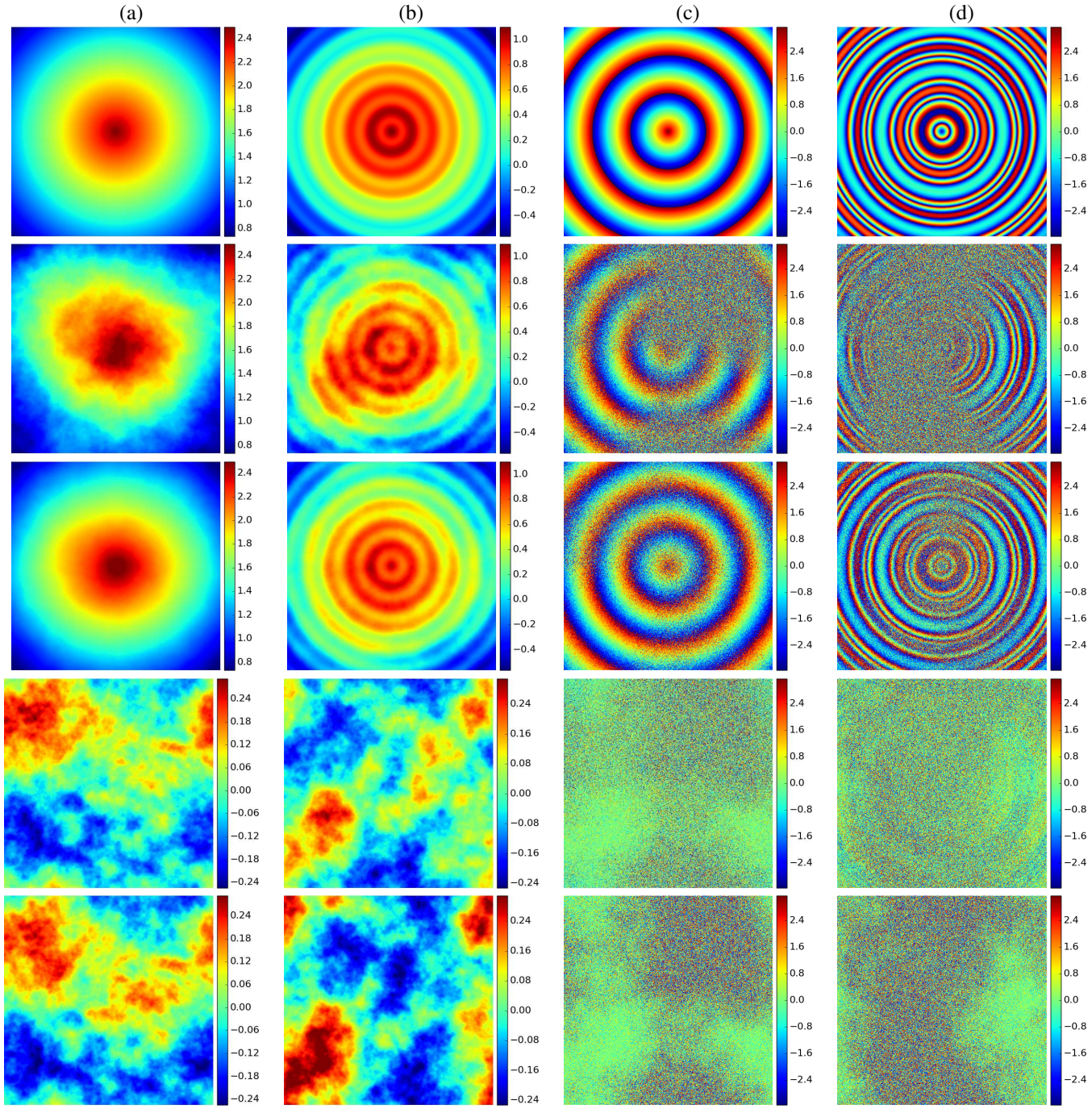


Fig. 8. Example of truth (first line), noisy displacement (second line), reconstruction (third line), residual (noisy displacement - reconstruction) (fourth line) and noise (fifth line) in case of (a) unwrapped interferogram of trend displacement (m) (b) unwrapped interferogram of oscillatory displacement (m) (c) wrapped interferogram of trend displacement (rad) (d) wrapped interferogram of oscillatory displacement (rad).

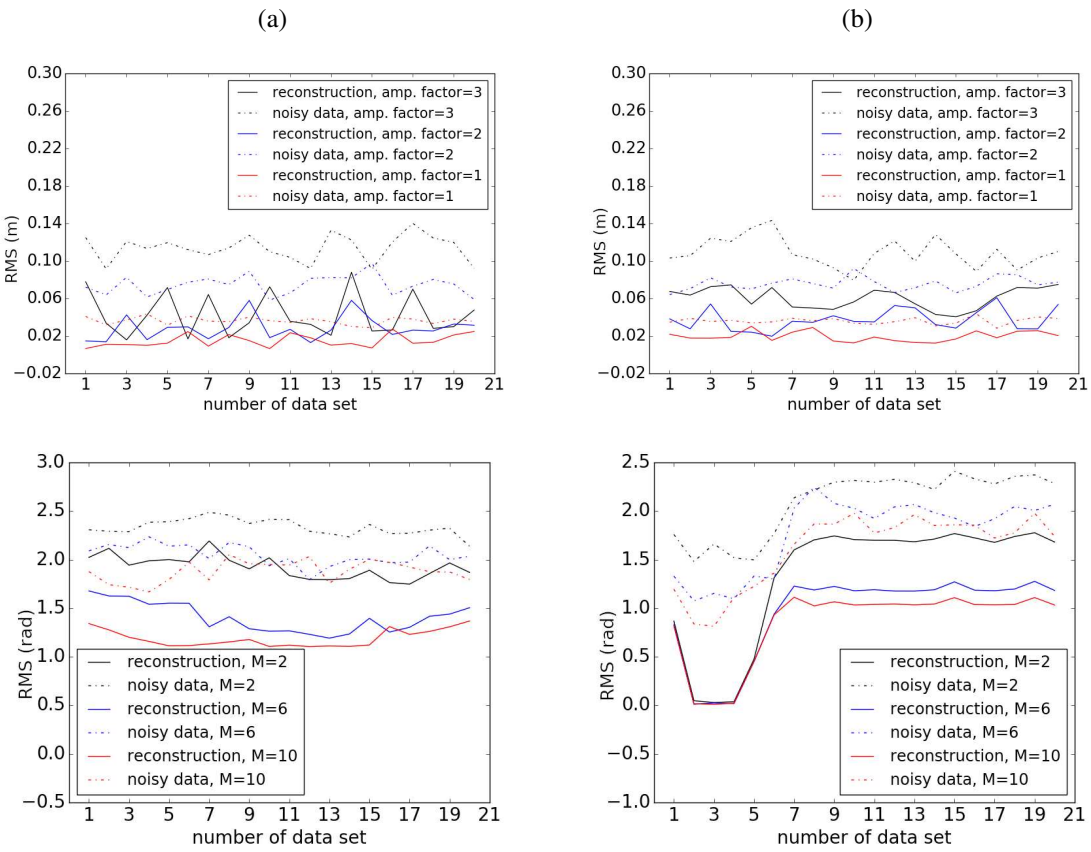


Fig. 9. Examples of RMS errors of the reconstruction (solid line) and noisy data (dashed line) for (a) trend displacement (b) oscillatory displacement in the case of unwrapped interferogram time series (top) and of wrapped interferogram time series (bottom). In case of wrapped interferogram time series, $M$ corresponds to the multi-looking factor in noise generation (see equation 28). In case of unwrapped interferogram time series, amp. factor corresponds to the amplification factor used in noise generation (see III-B).

generated in different cases. To introduce unique events in the time series, different displacement patterns have been used. For trend displacement time series, oscillatory displacement is used as unique events, while for oscillatory displacement time series, trend displacement is used as unique events. Thus, the displacement patterns of unique events are totally different from those in most other interferograms in the time series. The plot of the RMS errors of the reconstruction as a function of the number of interferograms with unique events is shown in Figure 11. In case of unwrapped interferograms of trend displacement (Figure 11 (a)), compared to the case without unique events, the RMS errors are only increased for interferograms with unique events. In other words, the reconstructions of other interferograms are not harmed by the unique events. Moreover, even with the presence of as many as 10 interferograms with unique events (given the total number of interferograms of 20), the RMS errors of other interferograms are not changed. In both cases of unwrapped interferograms of oscillatory displacement and wrapped interferograms of trend displacement (Figure 11 (b) and (c)), when the number of interferograms with unique events reaches as many as 5, the RMS errors of other interferograms begin to increase, while in case of wrapped interferograms of oscillatory displacement, the critical number of interferograms with unique events is 3. Therefore, given a limited number of both unwrapped and wrapped interferograms with unique events, the reconstructions of other interferograms can be not contaminated, the efficiency of the PM method can thus be maintained.

## IV. Application to Sentinel 1 interferogram time series for the Gorner glacier displacement measurement

In this section, a time series of 31 Sentinel-1 A/B images, acquired every 6 days between October 2016 and April 2017, covering the Gorner glacier situated at the frontier between Italy and Switzerland (Figure 12) is processed. 30 differential interferograms (after corrections of orbital and topographical contributions in the interferometric phase) are constructed from consecutive acquisitions, using a SRTM digital elevation model (DEM) (with a spatial resolution of 30 m) and auxiliary orbital data.

In the interferogram time series, the data quality is not homogeneous, because of the surface change (snow fall) from one acquisition to another. The quality of the data, indicated by the spatially averaged coherence, is presented in Figure 13. 11 out of 30 are of ”good” quality (fringe patterns are clearly visible over the whole glacier), with the averaged coherence larger than 0.35. 7 out of 30 are of ”moderate” quality, i.e. fringe patterns are visible over part of the glacier or over the whole glacier but with significant noise. The effective size

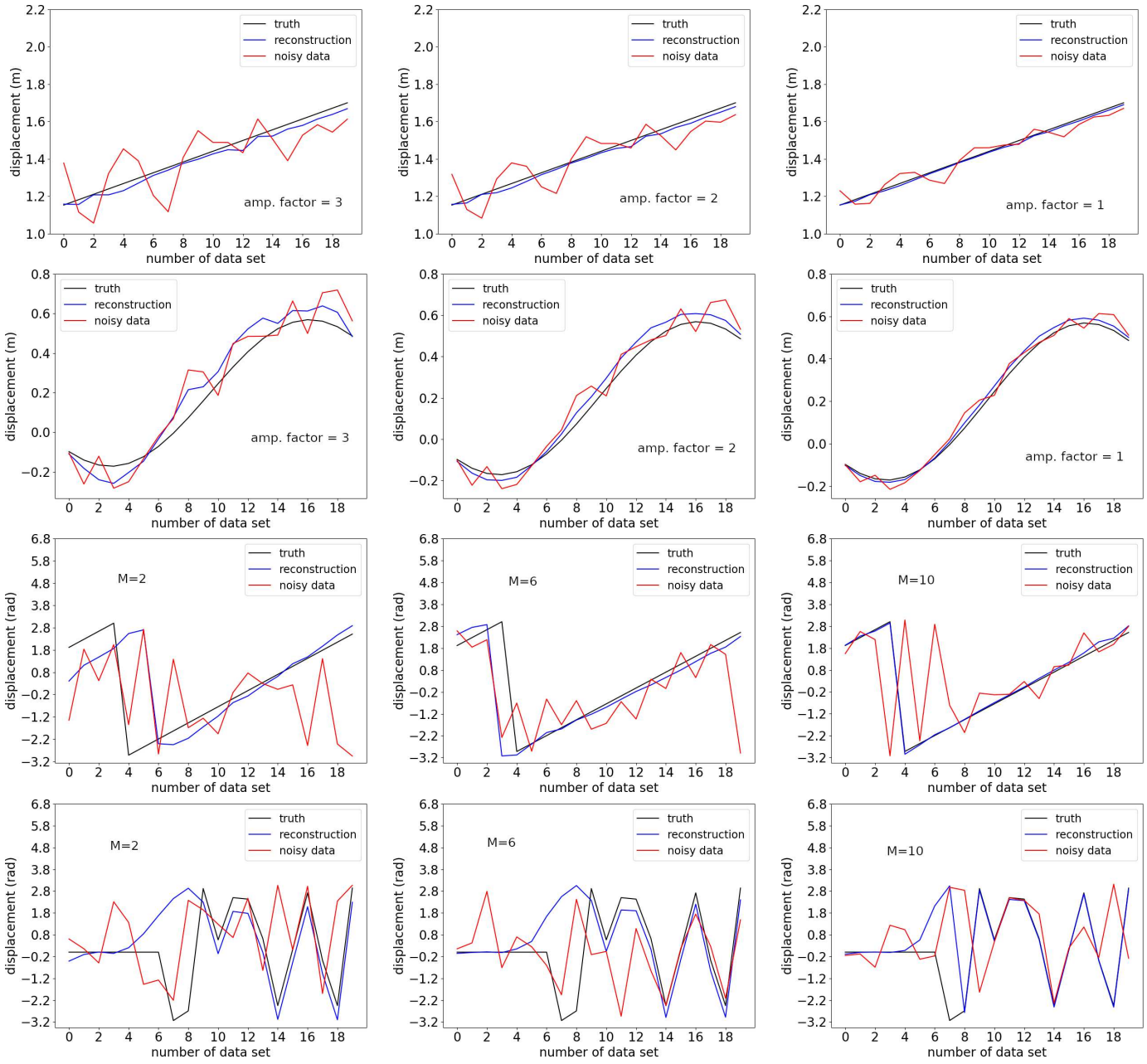


Fig. 10. Examples of displacement time series in case of different SNR for unwrapped interferogram time series (2 first lines) and wrapped interferogram time series (2 last lines). The first and third lines correspond to the trend displacement, and the second and fourth lines to the oscillatory displacement. $M$ corresponds to the multi-looking factor in noise generation (see equation (28)) and amp. factor corresponds to the amplification factor used in noise generation (see III-B). For each line, the global noise level decreases from left to right.

of the time series is thus 18. For interferograms with low coherence, the phase values can be considered as noise (partially or completely). Phase unwrapping is performed on all interferograms, using the Miminum Cost Flow (MCF) method provided with Gamma software with coherence as quality map. After the phase unwrapping, a constant shift exists on the interferograms because of the phase ambiguity. To fix this, a constant (an averaged value in a $100 \times 200$ window far from the glacier) is removed from each unwrapped interferogram with the underlying idea that there is no displacement in the stable area. The PM method is applied to the whole time series of both unwrapped and wrapped interferograms. In case of wrapped interferograms, 3 modes are used for the reconstruction, while in case of unwrapped interferograms, 2 modes are used, based on the check of the quality of the reconstruction. These choices are also confirmed by the difference of squared RMSD presented in Section III. For this glacier, there is no displacement measurements other than those from SAR interferometry. Indeed, the same problem exists for many other natural targets that present difficulties and risks to access for in situ instrumentation. Therefore, an absolute precise validation is not possible in the present study. Hence, we follow the common approach in displacement measurement without ground truth, that is, to check the residual

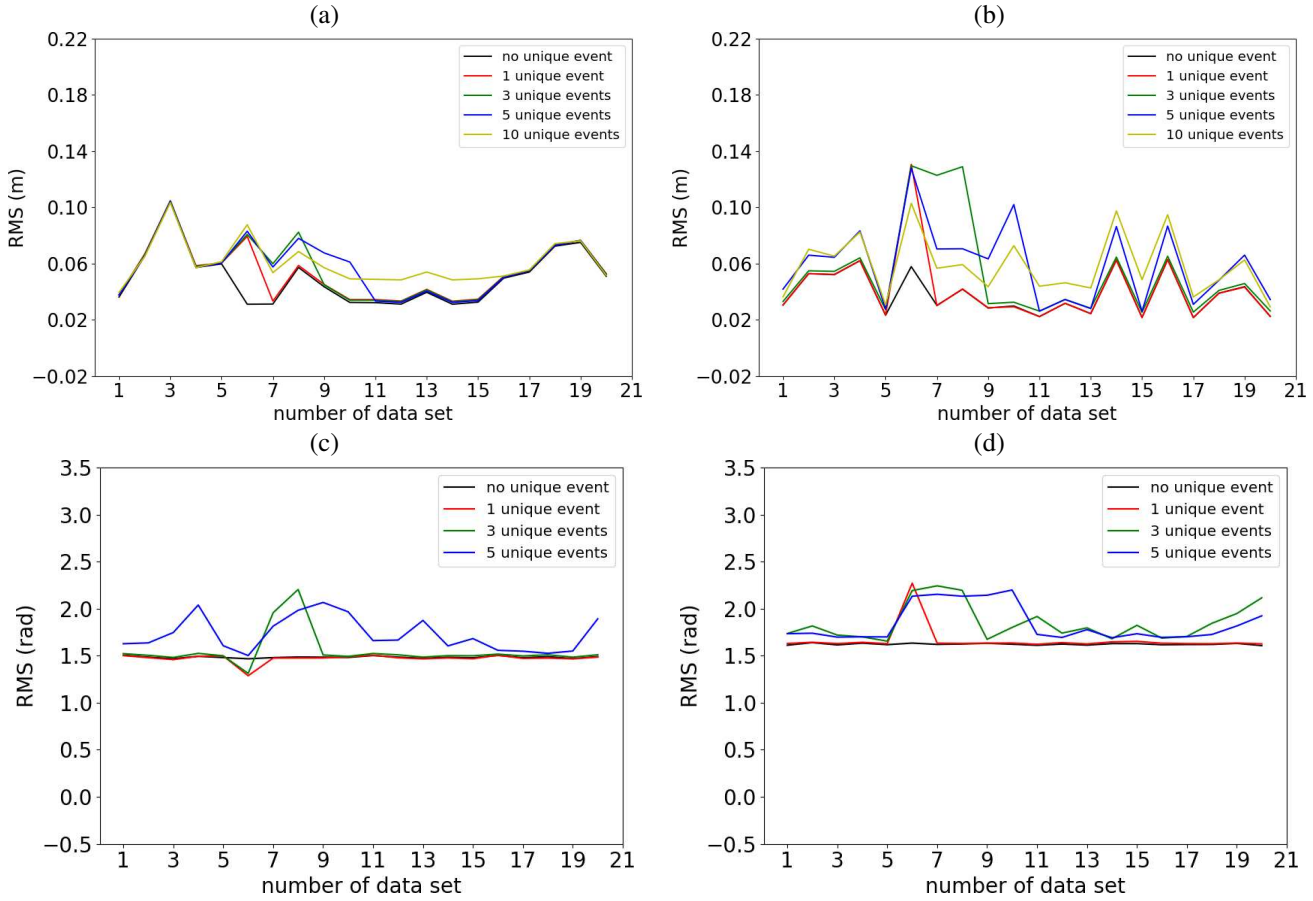


Fig. 11. Impact of unique events (whose displacement pattern is different from those in most interferograms in the time series) on the efficiency of the PM method in case of (a) unwrapped interferograms of trend displacement (b) unwrapped interferograms of oscillatory displacement (c) wrapped interferograms of trend displacement (d) wrapped interferograms of oscillatory displacement. Unique events exist from the $6^{th}$ data set and are continuous if the number is more than one. Unique events are oscillatory displacement for trend displacement time series and trend displacement for oscillatory displacement time series.

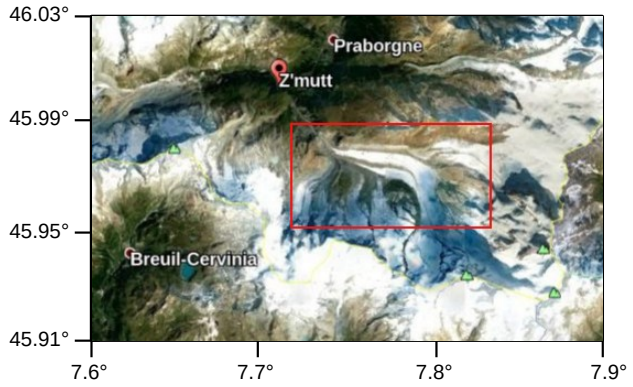


Fig. 12. Localisation of the Gorner glacier ($45.97°N, 7.8°E$, indicated by the black rectangle) at the frontier between Italy and Switzerland (Google Earth).

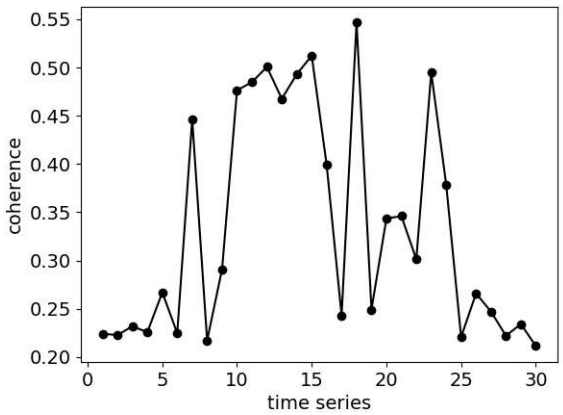


Fig. 13. Spatially averaged coherence of interferogram time series for displacement measurement over the Gorner glacier between October 2016 and April 2017.

(reconstructed interferograms - original interferograms). Note however that this residual, revealing how much an original interferogram is modified in the reconstruction by the PM method, is not an absolute indicator of the quality of the reconstruction, because it also depends on the quality of the original interferogram and the consistency of displacement behaviours between interferograms in the time series. The most important interest of the residual check lies on the verification if displacement signal is left in the residual.

The results in case of unwrapped interferograms are

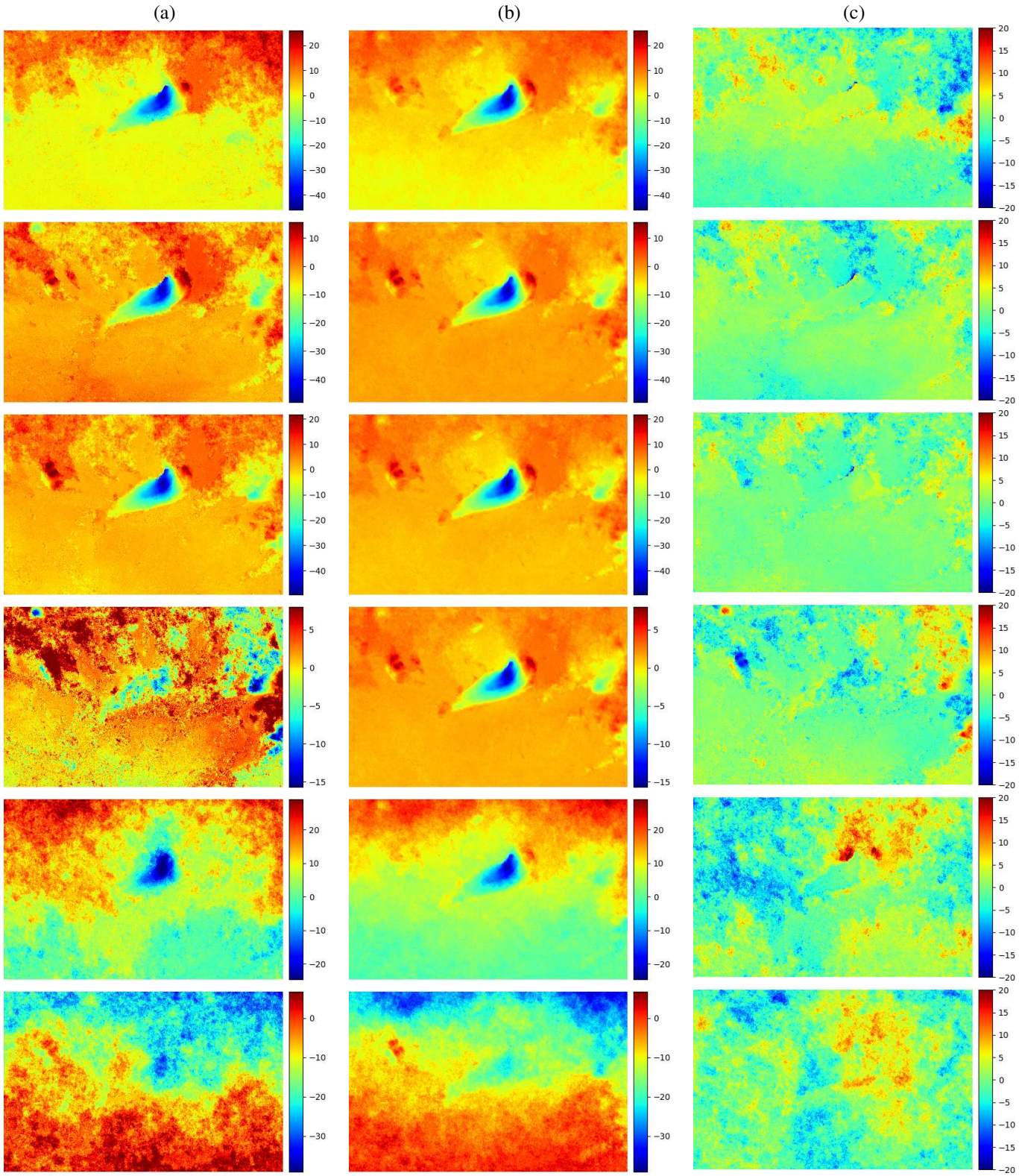


Fig. 14. (a) original and (b) reconstructed unwrapped interferograms (c) residual (reconstruction - original) at time spans (from top to bottom) 2016/12/17 - 2016/12/23, 2016/12/29 - 2017/01/04, 2017/02/15 - 2017/02/21, 2017/03/11 - 2017/03/17, 2017/02/03 - 2017/02/09, 2017/03/05 - 2017/03/11).

presented in Figure 14 with several representative examples. The original interferograms (2016/12/17 - 2016/12/23), (2016/12/29 - 2017/01/04) and (2017/02/15 - 2017/02/21) (first three lines in Figure 14) are already of good quality. The reconstructed interferograms can be considered as a filtered version of the original interferograms, with the displacement pattern over the glacier smoothed and most spatially correlated (at small scales) noise in stable areas filtered out (perturbations correlated at large scales and the displacement signal are mainly located at the two first EOF modes, thus impossible to separate them). The latter can also be observed from the residuals (Figure 14 (c)). The residuals over the glacier of these three interferograms are small and particularly homogeneous, with no clear displacement signal observed. Larger residuals are only observed at the upper edge of the glacier where localised phase unwrapping errors exist in the original interferograms due to the transition between the fast moving glacier and the stable areas. According to the histograms of residuals (Figure 15 (a) - (c)), the distributions of residuals are almost centred at 0 in stable areas. Over the glacier, a distribution centre shift from 0 is observed, especially for the interferogram (2016/12/17 - 2016/12/23). The mean residual values over the glacier are 1.14 cm, -0.34 cm and -0.05 cm respectively for these three interferograms (Table II). Thus, the relatively larger residual observed on the interferogram (2016/12/17 - 2016/12/23) is on the order of 1 cm. Note also that this larger residual is homogeneous over the glacier and it can be due to imperfect constant shift correction on unwrapped interferograms before the application of the PM method. A precise constant shift correction after phase unwrapping is expected to further improve the results of the PM method. For interferograms (2017/03/11 - 2017/03/17) and (2017/02/03 - 2017/02/09) ($4^{\text{th}}$ and $5^{\text{th}}$ lines in Figure 14), the original interferograms are sufficiently noisy, the displacement patterns are visible but significantly deformed. The PM method provides an important improvement: the deformation of the displacement pattern is corrected and a displacement pattern similar to those observed on interferograms of good quality is retrieved. Moreover, given larger noise in stable areas in the original interferograms, larger residuals are observed in stable areas for these two interferograms, which implies that the PM method is able to filter out most perturbations (correlated at small scales). The histograms of residuals (Figure 15 (d) - (e)) show that more larger residuals exist for these two interferograms compared to interferograms of good quality. This is due to significant correction of the displacement pattern over the glacier and efficient filtering of noise in stable areas in the reconstructions by the PM method. The original interferogram (2017/03/05 - 2017/03/11) (last line in Figure 14) is so noisy that it cannot provide any useful displacement information. After the PM method, the reconstructed interferogram is still very noisy, although the displacement pattern is highlighted. The residual is large, especially over the glacier (Figure 15 (f)), due to significant correction of displacement pattern on the reconstructed interferogram. The summary of residuals of all interferograms in the time series can be found in Table II. Over the glacier, most mean residual values are small, less than 1 cm. Displacement signal (of low magnitude) is identified in part of the glacier only on the interferogram (2016/12/05 - 2016/12/11), where a mean residual value of -1.27 cm is observed. These results show that, in case of unwrapped interferogram time series, 1) the PM method does not degrade interferograms of good quality, except the smoothness of the displacement pattern; 2) the good performance of the PM method is obtained for interferograms with a minimum sufficient SNR. Moreover, given the observation that localised phase unwrapping errors presented on a small proportion of interferograms can be filtered out, the PM method prefers local propagation phase unwrapping methods to global fit phase unwrapping methods.

In Figure 16, the results in case of wrapped interferograms are presented with several representative examples. The 6 interferograms are those in Figure 14 before phase unwrapping. The global observation is that fringe patterns are highlighted by the PM method for all interferograms, independent of the SNR. For interferograms (2016/12/17 - 2016/12/23) and (2016/12/29 - 2017/01/04) (first two lines in Figure 16), the PM method acts as a slight denoising filter. The residuals (modulo $2\pi$) confirm the quality of the reconstructed interferograms. Indeed, similar observations are obtained for most other interferograms of good quality in the time series. However, for the interferogram (2017/02/15 - 2017/02/21) (third line in Figure 16), large displacement signal is observed over the glacier in the residual. In fact, the fringe pattern of this interferogram is different from those on most other interferograms, i.e. one more fringe is observed on this interferogram. The reconstructed interferogram is similar to other interferograms. Consequently, large residual is observed. The PM method failed to capture the particular displacement behaviour (corresponding to unique event) on this interferogram. In the time series, the same problem also exists for the interferogram (2017/02/21 - 2017/02/27) that shares a common SAR image with the interferogram (2017/02/15 - 2017/02/21). These observations showcase a weakness of the PM method: with a certain number of modes retained in the reconstruction to eliminate as much as possible the noise, it happens that the reconstruction cannot capture high frequency displacement signal that represents unique events in the time series. For this, more modes are necessary in the reconstruction to keep this part of information, at the expense of keeping more noise at the same time. Another approach to get this part of information consists of a further analysis of the residual. Moreover, for interferograms (2016/11/29 - 2016/12/05) and (2017/01/04 - 2017/01/10) (not shown here), displacement signal is also observed in the residual, but the magnitude is smaller (less than one fringe). For interferograms (2017/03/11 - 2017/03/17), (2017/02/03-2017/02/09) and (2017/03/05-2017/03/11) (last three lines in Figure 16), part of or the whole interferograms are buried in the decorrelation noise. Fringe patterns are reconstructed successfully by the PM method, given the quality of the original interferogram. Similar results are obtained for all other low SNR interferograms in the time series. The residuals of these interferograms are so noisy that they cannot be used to indicate the quality of the reconstructed interferograms. As all the interferograms cover the same season and the displacement behaviour is consistent in most interferograms

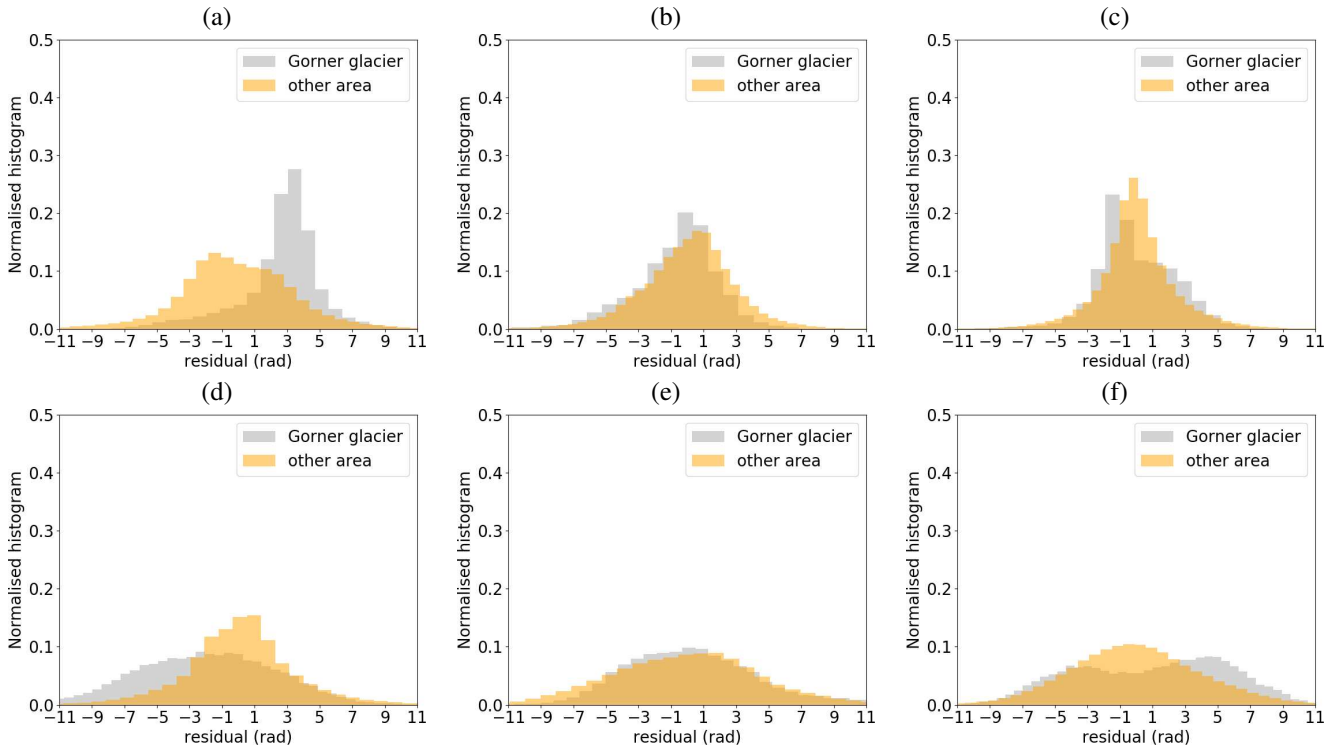


Fig. 15. Histograms of residual (shown in Figure 14 (c)) for (a) 2016/12/17-2016/12/23 (b) 2016/12/29 - 2017/01/04 (c) 2017/02/15 - 2017/02/21 (d) 2017/03/11 - 2017/03/17 (e) 2017/02/03-2017/02/09 (f) 2017/03/05-2017/03/11.

| N° | time span | unwrapped interferograms time series | | | | 2-stage PM application | | | |
|---|---|---|---|---|---|---|---|---|---|
| | | glacier | | stable area | | glacier | | stable area | |
| | | mean (cm) | std (cm) | mean (cm) | std (cm) | mean(cm) | std (cm) | mean (cm) | std (cm) |
| 1 | 2016/10/06 - 2016/10/12 | -0.73 | 1.70 | 0.04 | 1.36 | -0.14 | 1.54 | 0.26 | 1.4 |
| 2 | 2016/10/12 - 2016/10/18 | -0.36 | 1.57 | 0.02 | 1.45 | -5.42 | 3.68 | -0.55 | 1.55 |
| 3 | 2016/10/18 - 2016/10/24 | -0.09 | 1.89 | 0.00 | 1.64 | -1.76 | 4.22 | 1.26 | 2.41 |
| 4 | 2016/10/24 - 2016/10/30 | -0.51 | 1.63 | 0.03 | 1.58 | -8.34 | 5.20 | -2.05 | 2.71 |
| 5 | 2016/10/30 - 2016/11/05 | -1.39 | 1.66 | 0.07 | 1.64 | -2.10 | 2.01 | 0.48 | 1.73 |
| 6 | 2016/11/05 - 2016/11/11 | 0.53 | 1.72 | -0.02 | 2.00 | -5.66 | 5.79 | -1.18 | 2.26 |
| 7 | 2016/11/11 - 2016/11/17 | 0.37 | 1.22 | -0.02 | 1.33 | 0.17 | 1.62 | -0.03 | 1.55 |
| 8 | 2016/11/17 - 2016/11/23 | -0.33 | 1.61 | 0.02 | 1.99 | -4.40 | 4.76 | 0.38 | 2.05 |
| 9 | 2016/11/23 - 2016/11/29 | 0.46 | 2.38 | -0.02 | 1.79 | -3.85 | 4.58 | 0.11 | 2.23 |
| 10 | 2016/11/29 - 2016/12/05 | 0.06 | 1.03 | 0.00 | 1.22 | 0.68 | 1.58 | 0.70 | 1.81 |
| 11 | 2016/12/05 - 2016/12/11 | -1.27 | 1.00 | 0.06 | 1.42 | -1.22 | 1.45 | -0.67 | 1.94 |
| 12 | 2016/12/11 - 2016/12/17 | 0.11 | 1.19 | 0.00 | 1.57 | 0.18 | 1.57 | 0.39 | 1.84 |
| 13 | 2016/12/17 - 2016/12/23 | 1.14 | 1.20 | -0.06 | 1.55 | 0.14 | 1.75 | -1.61 | 2.27 |
| 14 | 2016/12/23 - 2016/12/29 | 0.18 | 1.28 | -0.01 | 1.16 | 0.03 | 1.79 | 0.49 | 1.61 |
| 15 | 2016/12/29 - 2017/01/04 | -0.34 | 1.27 | 0.02 | 1.27 | -0.42 | 1.58 | 0.10 | 1.39 |
| 16 | 2017/01/04 - 2017/01/10 | -0.66 | 1.40 | 0.03 | 1.36 | -2.20 | 1.79 | 0.21 | 1.79 |
| 17 | 2017/01/10 - 2017/01/16 | 0.20 | 1.86 | -0.01 | 1.56 | -5.91 | 5.42 | -0.54 | 1.73 |
| 18 | 2017/01/16 - 2017/01/22 | 0.24 | 1.40 | -0.01 | 1.37 | -0.08 | 1.50 | 0.14 | 1.28 |
| 19 | 2017/01/22 - 2017/01/28 | -1.07 | 1.45 | 0.05 | 1.46 | -3.83 | 2.36 | -0.36 | 1.47 |
| 20 | 2017/01/28 - 2017/02/03 | 0.81 | 1.30 | -0.04 | 1.58 | -2.78 | 2.53 | -0.71 | 1.90 |
| 21 | 2017/02/03 - 2017/02/09 | 0.42 | 2.25 | -0.02 | 2.03 | -5.34 | 2.86 | -3.42 | 3.38 |
| 22 | 2017/02/09 - 2017/02/15 | 0.83 | 1.71 | -0.04 | 1.60 | 0.20 | 3.80 | 2.84 | 2.25 |
| 23 | 2017/02/15 - 2017/02/21 | -0.06 | 1.14 | 0.00 | 1.05 | 1.51 | 2.23 | -0.20 | 1.34 |
| 24 | 2017/02/21 - 2017/02/27 | -0.41 | 1.60 | 0.02 | 1.29 | -1.11 | 2.45 | 0.38 | 1.73 |
| 25 | 2017/02/27 - 2017/03/05 | 0.19 | 1.66 | -0.01 | 1.61 | -6.99 | 2.96 | -3.24 | 2.77 |
| 26 | 2017/03/05 - 2017/03/11 | 0.40 | 2.06 | -0.02 | 1.77 | 3.16 | 5.34 | 6.13 | 5.09 |
| 27 | 2017/03/11 - 2017/03/17 | -0.87 | 1.88 | 0.04 | 1.52 | -4.40 | 5.13 | 0.56 | 1.82 |
| 28 | 2017/03/17 - 2017/03/23 | 0.15 | 1.62 | 0.00 | 1.89 | -7.10 | 5.73 | -1.11 | 2.39 |
| 29 | 2017/03/23 - 2017/03/29 | 0.68 | 1.62 | -0.03 | 1.64 | -6.55 | 5.44 | -1.18 | 2.08 |
| 30 | 2017/03/29 - 2017/04/04 | 0.16 | 1.35 | -0.01 | 1.64 | -3.97 | 5.49 | 1.50 | 2.30 |

TABLE II

MEAN AND STANDARD DEVIATION OF RESIDUALS (RECONSTRUCTED INTERFEROGRAMS - ORIGINAL INTERFEROGRAM) IN CASE OF UNWRAPPED INTERFEROGRAM TIME SERIES AND 2-STAGE APPLICATION OF THE PM METHOD. GRAY LINES CORRESPOND TO INTERFEROGRAMS OF GOOD QUALITY, WITH AVERAGED COHERENCE LARGER THAN 0.35.

of good quality, we can think that the displacement behaviour on these low SNR interferograms is also consistent with those observed on most interferograms of good quality. Therefore, the reconstructed interferograms can be considered credible. These results confirm the ability of the PM method to restore coherent fringe patterns in a wrapped interferogram time series including low or even very low SNR interferograms. In this way, useless interferograms can become exploitable, the PM method can thus increase the effective size of the time series.

According to the results of the interferograms of low SNR (2017/03/11 - 2017/03/17), (2017/02/03 - 2017/02/09) and (2017/03/05 - 2017/03/11), the PM method is more efficient in case of wrapped interferogram time series. Indeed, in this case, the phase value is modulo $2\pi$, in case of low SNR, the phase value includes only the decorrelation noise, the displacement signal is totally lost. The decorrelation noise is random, it does not introduce new variation directions in the SVD analysis of the temporal covariance matrix. While in case of unwrapped interferogram time series, even with low SNR, the displacement signal is still there, but biased significantly by the spatially correlated perturbations. This can hinder the true variation directions in the SVD analysis. Therefore, the PM method is more efficient in case of wrapped interferogram time series.

Given the efficiency of the PM method in denoising and reconstructing the fringe patterns on wrapped interferograms, it seems interesting to first apply the PM method on wrapped interferogram time series, and then to perform the phase unwrapping on interferograms with improved SNR, finally to apply a second time the PM method to unwrapped interferogram time series in order to separate the displacement signal from other spatially correlated perturbations. This processing strategy provides spectacular results. In Figure 17, the original unwrapped interferograms, the unwrapped reconstructed wrapped interferograms and the reconstruction after the 2-stage PM method are shown. The global observation for the 6 interferograms (as well as for other interferograms not shown) is that the displacement pattern over the glacier is highlighted and regularised and most perturbations (both at small and large scales) in stable areas are filtered out on the reconstructed interferograms after the 2-stage PM method. Important displacement signals have been retrieved successfully on almost useless original interferograms and perturbations correlated at large scales have been filtered out efficiently, thanks to the application of the PM method to the wrapped interferogram time series. Then a second application of the PM method to the unwrapped interferogram time series further removes the artefacts, which results of homogeneous, close to 0 values in stable areas (corresponding to the reality). The residuals (reconstructed interferogram after the 2-stage PM method (Figure 17 (c)) - unwrapped original interferogram (Figure 17 (a)) of the 6 reconstructed interferograms are shown in Figure 18 and the corresponding histograms are shown in Figure 19. For interferograms of good quality, in stable areas, the perturbations correlated at large scale (in the upper part of the image) in the original interferograms have been filtered to the residuals, which results of larger residuals compared to the case of unwrapped interferograms (see also Table II). Over the glacier, the first observation is the large residual at the upper edge of the glacier due to localised phase unwrapping errors in the original unwrapped interferogram (see also first three lines of Figure 14 (c)). Displacement signal is observed in the residual of the interferogram (2017/02/15 - 2017/02/21) (Figure 18 (c)), consistent with the large distribution centre shift observed in Figure 19 (c), because of the inappropriate modification of the fringe pattern on the wrapped interferogram by the PM method. For interferograms (2016/12/17-2016/12/23) and (2016/12/29 - 2017/01/04) (Figure 18 (a) (b), Figure 19 (a) (b)), the residuals are small and homogeneous, with mean values of 0.14 cm and -0.42 cm respectively (Table II). For interferograms of low SNR (2017/03/11 - 2017/03/17), (2017/02/03-2017/02/09) and (2017/03/05-2017/03/11) (Figure 18 (d)-(f), Figure 19 (d)-(f)), the observations are similar: over the glacier, large residuals are mainly due to significant corrections of the displacement pattern (noise replaced by coherent displacement signal) by the PM method; while in stable areas, perturbations spatially correlated at both small and large scales in the original interferograms have most been filtered to the residuals. The summary of residuals of all interferograms in the time series can be found in Table II. Compared to the case of unwrapped interferograms, the increased mean residual values in stable areas imply the efficiency of the 2-stage PM method in filtering perturbations spatially correlated both at small and large scales. Over the glacier, for interferograms of low SNR, larger residuals are due to significant correction of the displacement pattern in the reconstruction; for interferograms of good quality, most mean residual values are decreased or stay the same, which indicates the improvement of the 2-stage PM method compared with the only application to unwrapped interferograms. Larger residual exists for interferograms where larger residual is obtained on reconstructed wrapped interferograms due to non coherent displacement signals (i.e. unique events) on these interferograms.

To further validate the reconstructions of the PM method, offset tracking is applied to Sentinel-1 image pairs of 12-days interval in order to obtain other type of displacement measurement as in [28]. The mean velocity over the Gorner glacier obtained from 7 offset tracking measurements of good quality is shown in Figure 20 (a). Except some artifacts at the edge of the glacier, the displacement pattern is similar to that observed in interferograms. This mean velocity is compared to those obtained from original interferograms, reconstructed unwrapped interferograms and reconstructions of the 2-stage application of the PM method on a profile located along the central line of the glacier (Figure 20). Original interferograms and reconstructed unwrapped interferograms underestimate the mean velocity in areas where the glacier flow velocity is largest. The mean velocity obtained from the 2-stage application of the PM method follows well that issued from offset tracking measurements, which confirms the efficiency of the 2-stage PM method.

## V. Connection to other multi-temporal InSAR approaches

The PM method can improve the SNR of interferograms, therefore, it is expected that using the reconstructed interfero-

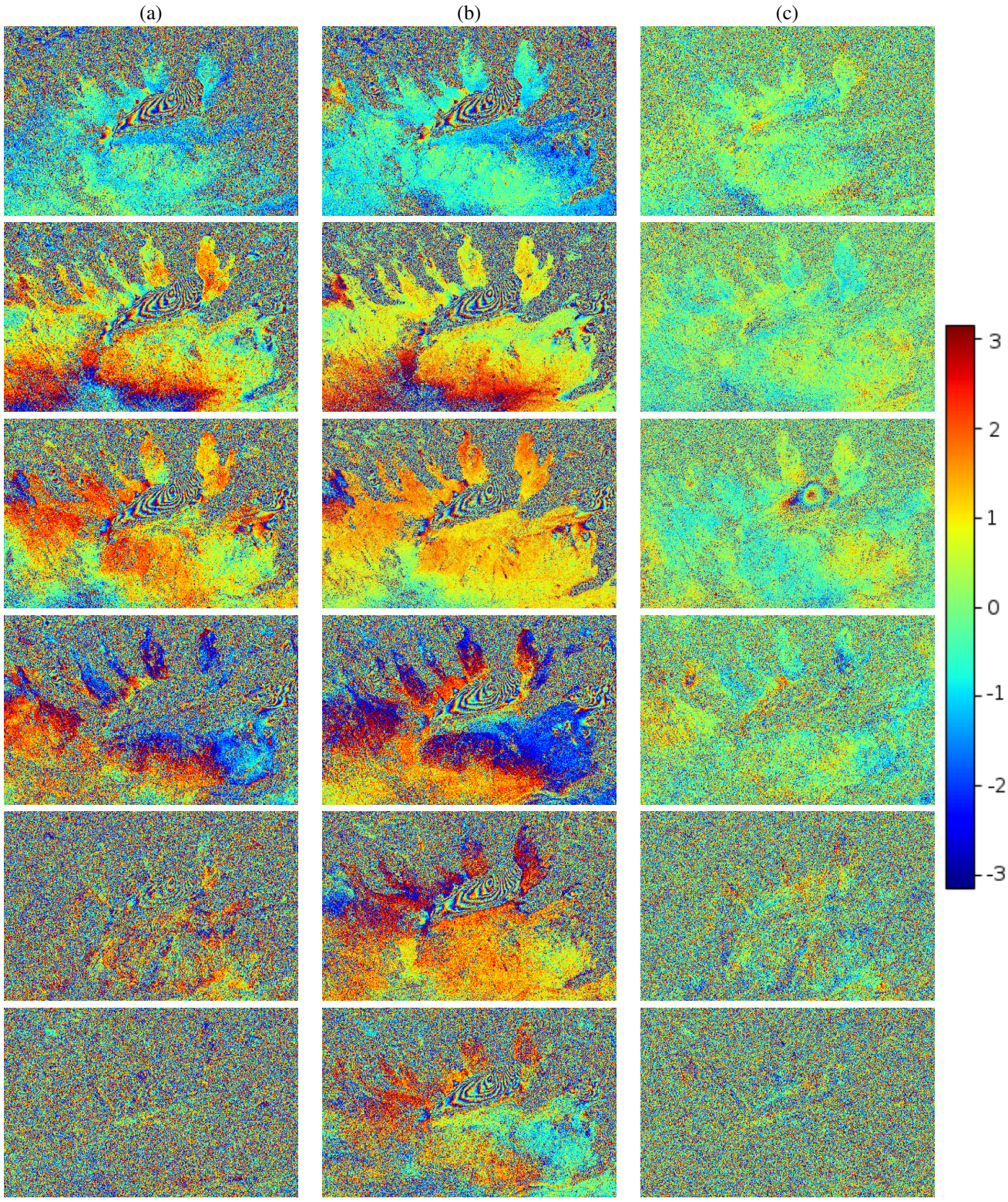


Fig. 16. (a) original (b) reconstructed wrapped interferograms (c) residual (reconstruction - original) modulo $2\pi$ at time spans (from top to bottom) 2016/12/17 - 2016/12/23, 2016/12/29 - 2017/01/04, 2017/02/15 - 2017/02/21, 2017/03/11 - 2017/03/17, 2017/02/03 - 2017/02/09, 2017/03/05 - 2017/03/11).

grams by the PM method in other multi-temporal approaches can further improve the final accuracy of displacement rate estimation. This seems particularly useful in case of interferograms of moderate to low SNR, where other multi-temporal approaches alone cannot work due to coherence loss. In the present application of the PM method, interferograms from consecutive SAR acquisitions (i.e. very small temporal baseline) are used. The use of these reconstructed interferograms in

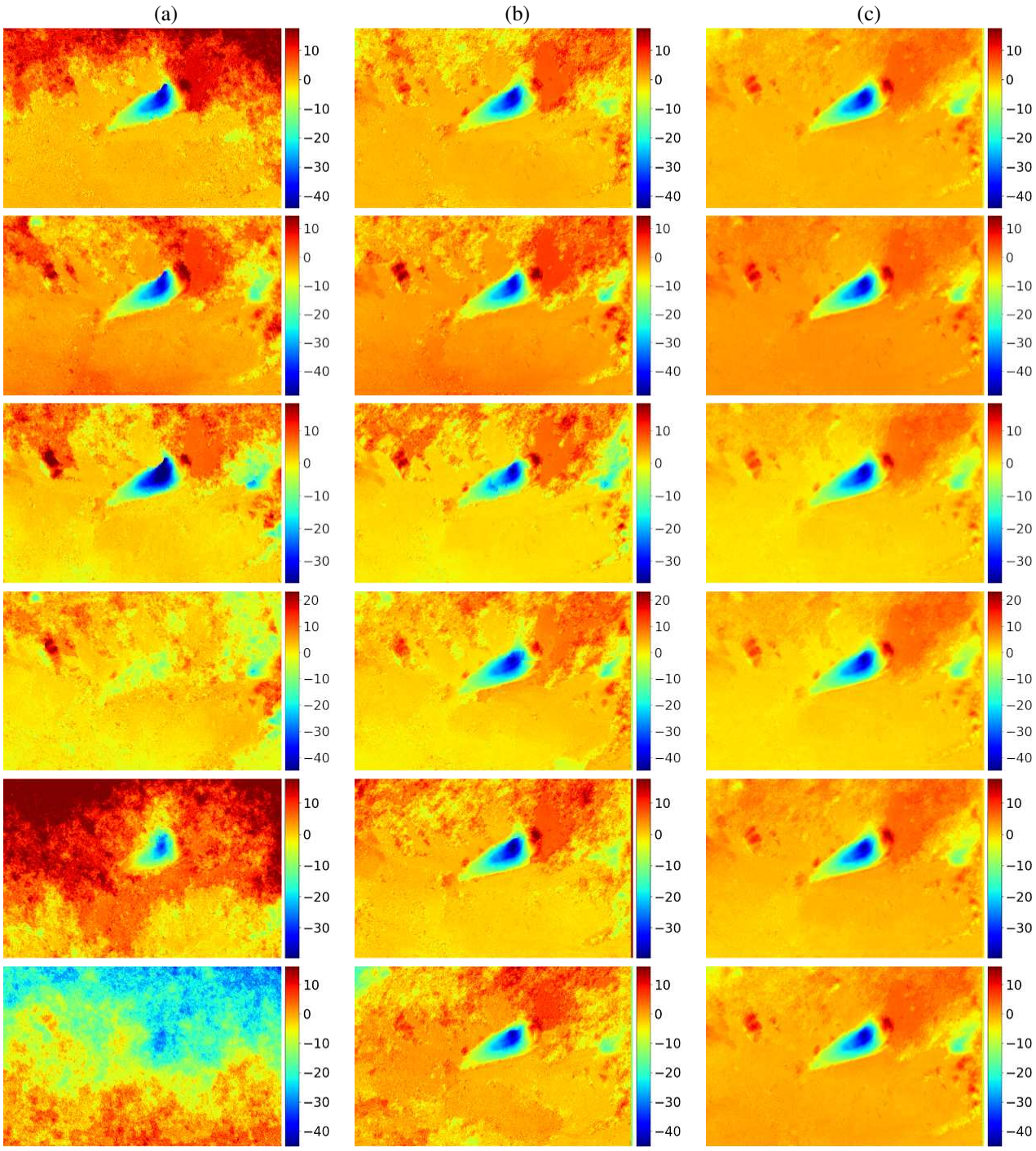


Fig. 17. (a) Original unwrapped interferograms (b) unwrapped interferogram of the PM wrapped reconstruction (c) reconstruction of the 2-stage PM method at time spans (from top to bottom) 2016/12/17 - 2016/12/23, 2016/12/29 - 2017/01/04, 2017/02/15 - 2017/02/21, 2017/03/11 - 2017/03/17, 2017/02/03 - 2017/02/09, 2017/03/05 - 2017/03/11).

other mutli-temporal approaches will not be beneficial because of lack of redundancy in the interferogram network. Indeed, single master interferograms time series can also be used in the PM method and single master interferograms time series is often used in PS approaches. Thus, it is interesting to investigate the gain in accuracy by using the reconstructed single master interferograms time series in a PS approach. For a full stack of all possible interferograms from a time series of SAR images, these interferograms cannot be used together directly in the PM method. In this case, it is better to first reorganise all interferograms into several single master or equal temporal baseline interferogram groups. Then, the reconstruction can be performed in each group in order to make use of the PM method to improve the SNR. Afterwards, the reconstructed interferograms can be used in other multi-temporal approaches in order to make the application of the

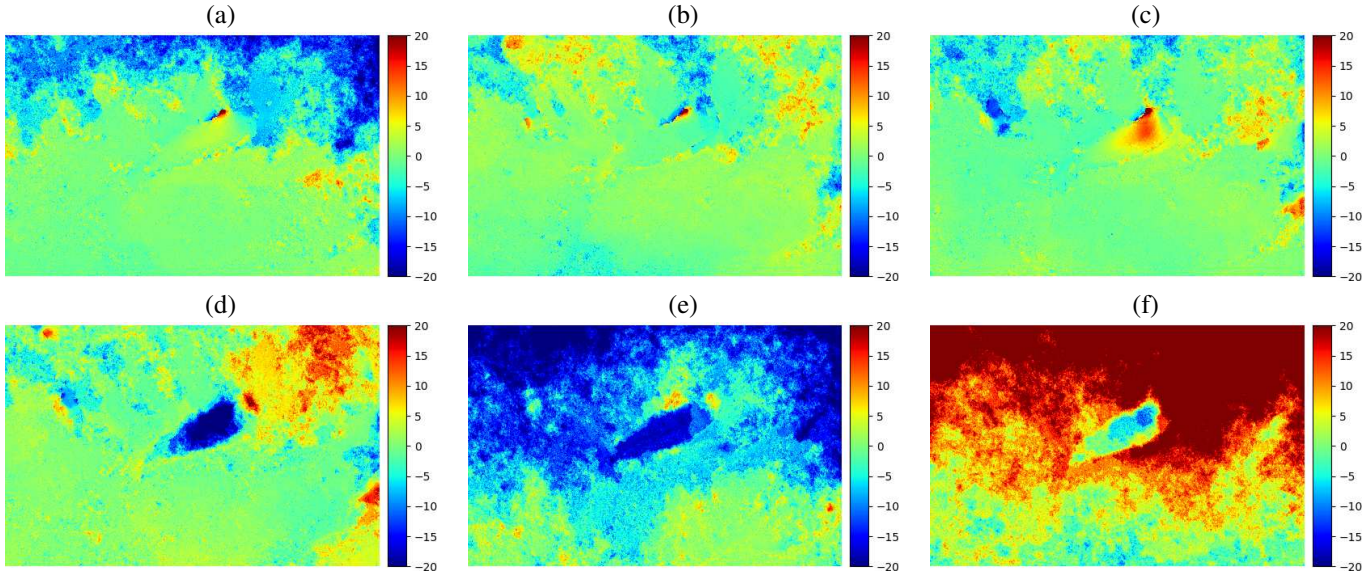


Fig. 18. Residual (unwrapped interferogram after the 2-stage PM method (i.e. Figure 17 (c)) - original unwrapped interferogram (i.e. Figure 17 (a)) for (a) 2016/12/17-2016/12/23 (b) 2016/12/29 - 2017/01/04 (c) 2017/02/15 - 2017/02/21 (d) 2017/03/11 - 2017/03/17 (e) 2017/02/03-2017/02/09 (f) 2017/03/05-2017/03/11 2016/12/17-2016/12/23.

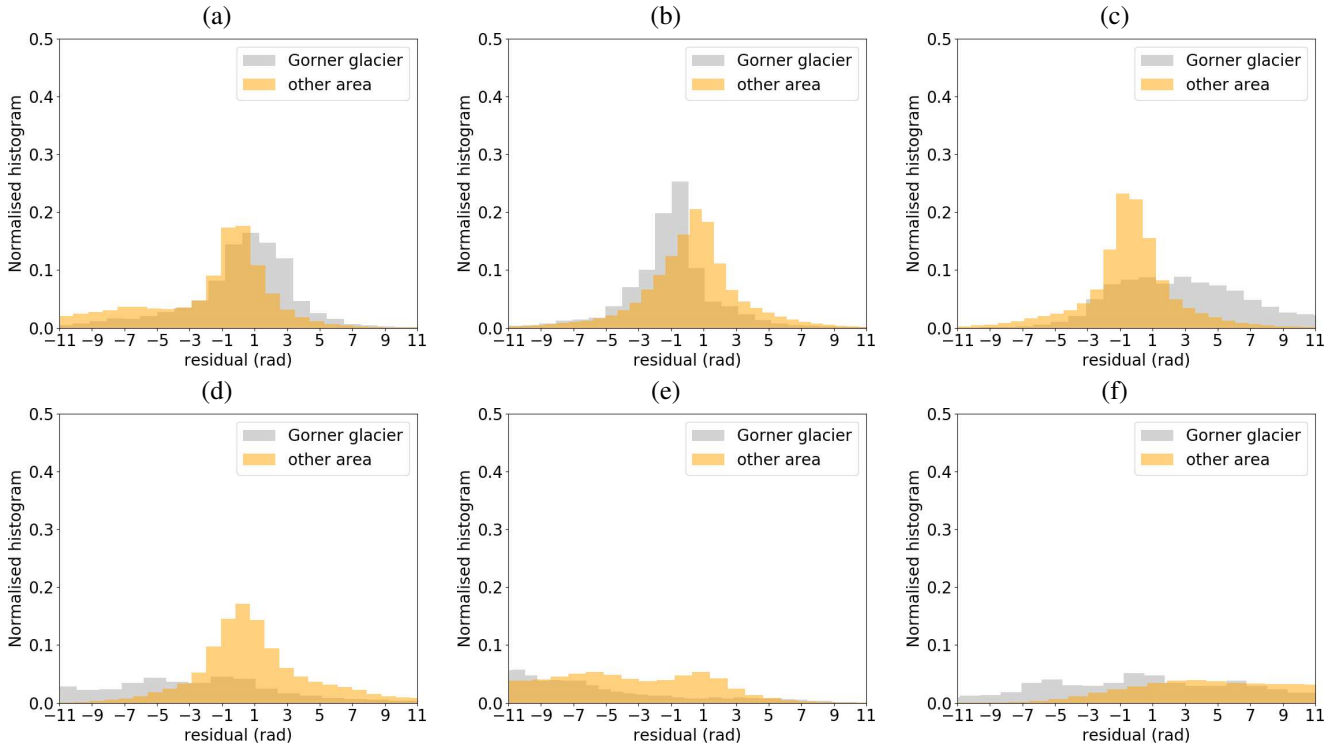


Fig. 19. Histograms of residual (shown in Figure 18) for (a) 2016/12/17-2016/12/23 (b) 2016/12/29 - 2017/01/04 (c) 2017/02/15 - 2017/02/21 (d) 2017/03/11 - 2017/03/17 (e) 2017/02/03-2017/02/09 (f) 2017/03/05-2017/03/11.

latter possible and to improve the accuracy of displacement rate estimation.

## VI. Conclusion

In this paper, a data-adaptive method, the PM method, based on a SVD analysis of the spatially averaged temporal covariance of a time series, is proposed to retrieve coherent displacement signal from a displacement measurement time series from consecutive SAR acquisitions for decorrelating targets. The PM method learns about the underlying processes that control the evolution of the time series and identifies the spatial patterns that vary together following a specific time function. Thereby, it can separate the coherent displacement signal and other perturbations in a displacement measurement

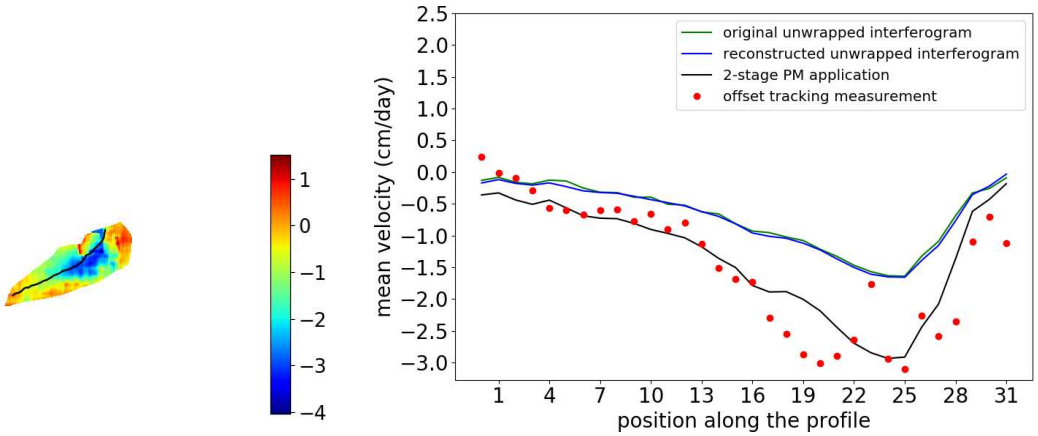


Fig. 20. (a) Mean velocity (cm/day) over the Gorner glacier obtained from 7 offset tracking measurements (from Sentinel-1 image pairs of 12-days interval) of good quality between 2016/11/29 and 2017/02/27 (b) Mean velocities on the profile indicated by a black line in (a) obtained from all original interferograms, reconstructed unwrapped interferograms, reconstructions of the 2-stage application of the PM method and 7 offset tracking measurements of good quality.

time series. In a time series of displacement measurement, for high SNR data sets, it behaves like a filter that denoises the displacement patterns, while for low SNR data sets, it can be considered as a gap filler that replaces the noise by coherent displacement signal based on the spatial and temporal correlation of the displacement. The PM method can be applied to both wrapped and unwrapped interferogram time series. In both applications, it is demonstrated that the PM method has strong capacity in retrieving coherent signals in the time series with low SNR. For decorrelating targets, the PM method, especially the 2-stage PM method, can make useless data exploitable thus increase the effective size of the displacement time series, which is important to provide complete and credible information about the evolution of the phenomenon under observation.

Besides the high efficiency, the PM method presents other advantages, for instance, it does not need any a priori knowledge about the displacement characteristics. Moreover, since it works with the data alone, inhomogeneities and/or non-isotropic behaviours are automatically taken into account in the processing. Furthermore, the ease of implementation constitutes another important feature of the PM method, which makes it possible to be considered as a routine method for displacement signal retrieval from a time series.

On the other hand, the PM method also presents some limitations. It is particularly suitable for measurement of continuous displacement over time (linear, with acceleration/deceleration, periodic, etc). In other words, primary variation modes must exist in the SVD analysis of the temporal covariance. For significantly irregular displacement (e.g. intermittent or random displacement), the PM method may fail, due to lack of dominant variability in the time series. Moreover, in case of regular displacement, if high frequency displacement related to unique events exists in the time series, it can be lost in the reconstruction. Further analysis on the residual will be necessary to retrieve this part of displacement.

The PM method works with very simple assumptions, i.e. the displacement pattern is continuous and coherent over time, while other perturbations are not. This corresponds to most cases in real displacement measurement. However, more complex displacement and perturbation behaviours could happen in some cases. For this, an extension of the PM method taking into account also the spatial covariance, thus the spatio-temporal covariance will be investigated in the future work. Furthermore, the combination of the PM method and other multi-temporal InSAR approaches in case of moderate to high SNR also constitutes a promising subject to investigate in the future work.

## ACKNOWLEDGMENT

The authors would like to thank all anonymous reviewers for their comments and suggestions.

## REFERENCES

[1] K. Dai, Z. Li, R. Tomas, G. Liu, B. Yud, X. Wang, H. Chenge, J. Chen, and J. Stockamp, "Monitoring activity at the daguangbao mega-landslide (china) using sentinel-1 tops time series interferometry," *Remote Sensing of Environment*, vol. 186, pp. 501–513, 2016.

[2] S. Winsvold, A. Kääb, C. Nuth, L. Andreassen, W. van Pelt, and T. Schellenberger, "Using SAR satellite data time series for regional glacier mapping," *The Cryosphere Discussion*, 2017.

[3] V. Drouin, F. Sigmundsson, S. Verhagen, B. Ofeigsson, K. Spaans, and S. Hreinsdottire, "Deformation at krafla and bjarnarflag geothermal areas, northern volcanic zone of iceland, 1993–2015," *Journal of Volcanology and Geothermal Research*, vol. 344, pp. 92–105, 2017.

[4] W. Ahmad, M. Choi, S. Kim, and D. Kim, "Detection of land subsidence due to excessive groundwater use varying with different land cover types in quetta valley, pakistan using esa sentinel satellite data," *Nat. Hazards Earth Syst. Sci. Discuss.*, 2017.

[5] A. Ferretti, C. Prati, and F. Rocca, "Permanent scatterer in SAR interferometry," *IEEE Transactions on Geoscience and Remote Sensing*, vol. 39, no. 1, pp. 8–20, 2001.

[6] C. Werner, U. Wegmuller, T. Strozzi, and A.Wiesmann, "Interferometric point target analysis for deformation mapping," in *Geoscience and Remote Sensing Symposium*, vol. 7, pp. 4362–4364, 2003.

[7] A. Hooper, P. Segall, and H. Zebker, "Persistent scatterer interferometric synthetic aperture radar for crustal deformation analysis with application to Volcan Alcedo, Galapagos," *Journal of Geophysical Research*, vol. 112, no. B07407, 2007.

[8] A. Ferretti, A. Fumagalli, F. Novali, C. Prati, F. Rocca, and A. Rucci, "A new algorithm for processing interferometric data-stacks: SqueeSAR," *IEEE Transactions on Geoscience and Remote Sensing*, vol. 49, no. 9, pp. 3460–3470, 2011.

[9] R. Lanari, O. Mora, M. Manunta, J. Mallorqui, P. Berardino, and E. Sansosti, "A Small-Baseline Approach for Investigating Deformations on Full-Resolution Differential SAR Interferograms," *IEEE Transaction on Geoscience and Remote Sensing*, vol. 42, no. 7, pp. 1377–1386, 2004.
[10] A. Pepe, Y. Yang, M. Manzo, and R. Lanari, "Improved EMCF-SBAS processing chain based on advanced techniques for the noise-filtering and selection of small baseline multi-look DInSAR interferograms," *IEEE Transactions on Geoscience and Remote Sensing*, vol. 53, no. 8, pp. 4394–4417, 2015.
[11] G. Fornaro, S. Verde, D. Reale, and A. Pauciullo, "Caesar: An approach based on covariance matrix decomposition to improve multibaseline - multitemporal interferometric SAR processing," *IEEE Transactions on Geoscience and Remote Sensing*, vol. 53, no. 4, pp. 2050–2065, 2015.
[12] D. Perissin and T. Wang, "Repeat-pass SAR interferometry with partially coherent targets," *IEEE Transactions on Geoscience and Remote Sensing*, vol. 50, no. 1, pp. 271–280, 2012.
[13] F. Rocca, "Modelling interferogram stacks," *IEEE Transaction on Geoscience and Remote Sensing*, vol. 45, no. 10, pp. 3289–3299, 2007.
[14] A. M. Guarnieri and S. Tebaldini, "On the exploitation of target statistics for SAR interferometry applications," *IEEE Transaction on Geoscience and Remote Sensing*, vol. 46, no. 11, pp. 3436–3443, 2008.
[15] B. Pinel-Puysségur, R. Michel, and J. Avouac, "Multi-Link InSAR time series: Enhancement of a wrapped interferometric database," *IEEE Journal of Selected Topics in Applied Earth Observations and Remote Sensing*, vol. 5, no. 3, pp. 784–794, 2012.
[16] S. Samiei-Esfahany, J. E. Martins, F. van Leijen, and R. Hanssen, "Phase estimation for distributed scatterers in InSAR stacks using integer least squares estimation," *IEEE Transaction on Geoscience and Remote Sensing*, vol. 54, no. 10, pp. 5671–5687, 2016.
[17] H. Ansari, F. D. Zan, and R. Bamler, "Sequential estimator: Toward efficient InSAR time series analysis," *IEEE Transaction on Geoscience and Remote Sensing*, vol. 55, no. 10, pp. 5637–5652, 2017.
[18] Y. Wang and X. Zhu, "Robust estimators for multipass SAR Interferometry," *IEEE Transaction on Geoscience and Remote Sensing*, vol. 54, no. 2, pp. 968–980, 2016.
[19] R. Preisendorfer, *Principal Component Analyses in Meteorology and Oceanography*. Elsevier, 1988.
[20] J. Beckers and M. Rixen, "Eof calculations and data filling from incomplete oceanograhic datasets," *Journal of Atmospheric and Oceanic Technology*, vol. 20, no. 12, pp. 1839–1856, 2003.
[21] A. Hannachi, I. Jolliffe, and D. Stephenson, "Empirical orthogonal functions and related techniques in atmospheric sciences: A Review," *International Journal of Climatology*, vol. 27, pp. 1119–1152, 2007.
[22] C. Bretherton, C. Smith, and J. Wallage, "An intercomparison of methods for finding coupled patterns in climate data," *Journal of Climate*, vol. 5, no. 6, pp. 541 – 560, 1992.
[23] M. Ghil, M. Allen, M. Dettinger, K. Ide, D. Kondrashov, M. Mann, A. Robertson, A. Saunders, Y.Tian, F. Varadi, and P. Yiou, "Advanced spectral methods for climatic time series," *Review of Geophysics*, vol. 40, no. 1, pp. 3–1–3–41, 2002".
[24] A. Kositsky and J. Avouac, "Inverting geodetic time series with a principal component analysis-based inversion method," *Journal of Geophysical Research*, vol. 115, no. B03401, 2010.
[25] R. Preisendorfer and J. Overland, "A significant test for principal components applied to a cyclone climatology," *Monthly Weather Review*, vol. 110, pp. 1–4, 1982.
[26] T. Stozzi, U. Wegmuller, L. Tosi, G. Bitelli, and V. Spreckels, "Land subsidence monitoring with differential sar interferometry," *Photogrammetric Engineering and Remote Sensing*, vol. 67, no. 11, pp. 1261 – 1270, 2001.
[27] C. Willmott and K. Matsuura, "On the use of dimensioned measures of error to evaluate the performance of spatial interpolators," *International Journal of Geographic Information Science*, vol. 20, no. 1, pp. 89 – 102, 2006.
[28] T. Strozzi, A. Luckman, T. Murray, U. Wegmüler, and C. Werner, "Glacier motion estimation using sar offset-tracking procedures," *IEEE Transaction on Geoscience and Remote Sensing*, vol. 40, no. 11, pp. 2384–2391, 2002.

**Rémi Prébet** is actually a Master student in the department of Mathematics at École Normale Supérieure Paris-Saclay, France. He did his Master internship at Laboratoire d'Informatique, Systèmes, Traitement de l'Information et de la Connaissance (LISTIC).

**Yajing Yan** (M'17) received the M.S. degree in physical methods in remote sensing from University Paris 6, France, in 2008, and the Ph.D. degree in geosciences and environment from LISTIC and Institut des Sciences de la Terre (ISTerre) of University Savoie Mont-Blanc, France, in 2011. She was a Postdoc Fellow at Institut d'Électronique et des Télécommunications de Rennes (IETR) of University Rennes 1, France between Jan. 2012 and June 2012 and at GeoHydrodynamics and Environment Research of University of Liège, Belgium between July 2012 and August 2014. Since September 2014, she is an Associate Professor at LISTIC, University Savoie Mont-Blanc. Her research interests include multi-temporal SAR processing, data fusion and data assimilation.

**Matthias Jauvin** received the B.Eng. degree in geophysics from the French Engineering School "Ecole et Observatoire des Sciences de la Terre of Strasbourg" in 2015. He is currently working towards the Ph.D. degree at LISTIC lab. of Université Savoie Mont-Blanc, Annecy, France. His main work concerns surface deformation monitoring in both natural and urban areas by satellite SAR images. He is also a project manager of AURIGAMI company and involved in urban monitoring projects, working in collaboration with the LISTIC laboratory. His research interests include multi-temporal InSAR processing and integration of corner reflectors in InSAR time series analysis.

**Emmanuel Trouvé** (M'00–SM'10) received the Engineer degree in electrical engineering from the École Nationale Supérieure de Techniques Avancées, Paris, France, in 1990, the Ph.D. degree in signal and image processing from Ecole Nationale Supérieure des Télécommunications, Paris, France, in 1996, and the "Habilitation à Diriger des Recherches" degree from University Savoie Mont-Blanc, Chambéry, France, in 2006. From 1996 to 1998, he worked with Thomson Marconi Sonar in Underwater Acoustic and Signal Processing. He has been working with the lab. LISTIC, Polytech Annecy-Chambéry, University Savoie Mont Blanc, Annecy, France, as an Associate Professor (1998–2008), and then, as a Professor since 2008 and Director of the lab. LISTIC since 2018. His research interests include SAR image analysis and data fusion in remote sensing. He has coordinated several research projects, including the national multilaboratory project EFIDIR (Extraction and Fusion of Information for Displacement measurement from SAR Imagery, 2008–2012). He was the General Chair of the 8th International Workshop on the Analysis of Multitemporal Remote Sensing Images and the treasurer of the French Chapter of the IEEE Geoscience and Remote Sensing Society from 2013 to 2016.